
Article:
Borsellini, A., Conti, D., Cutts, E.E. orcid.org/0000-0003-3290-4293 et al. (20 more authors) (2025) Condensin II activation by M18BP1. Molecular Cell, 85 (14). 2688-2700.e11. ISSN 1097-2765

https://doi.org/10.1016/j.molcel.2025.06.014

Molecular Cell

Article

Condensin II activation by M18BP1

Graphical abstract

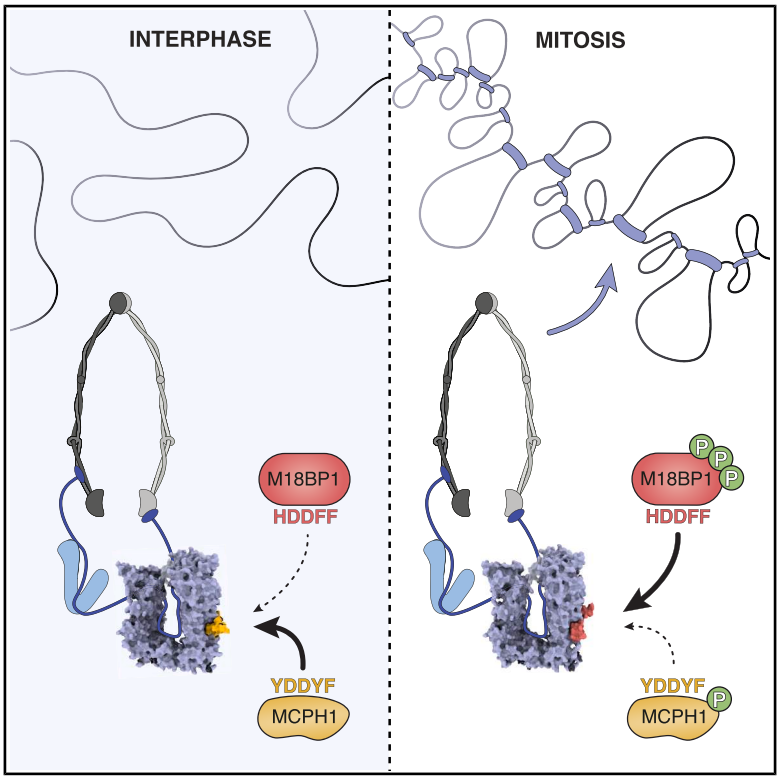

Authors

Alessandro Borsellini, Duccio Conti, Erin E. Cutts, ..., Benjamin D. Rowland, Andrea Musacchio, Alessandro Vannini

Correspondence

e.cutts@sheffield.ac.uk (E.E.C.), b.rowland@nki.nl (B.D.R.), andrea.musacchio@mpi-dortmund.mpg.de (A.M.), alessandro.vannini@fht.org (A.V.)

In brief

Borsellini, Conti, Cutts, Harris, et al. identify an interaction between M18BP1 and condensin II that is essential for condensin II activity and chromatin localization. MCPH1 keeps the interphase genome uncondensed by competing with M18BP1. A phosphorylation-driven switch allows M18BP1 to trigger condensation at mitotic onset.

Highlights

- M18BP1 is crucial for condensin II activity in human cells
- Condensin II's CAP-G2 subunit directly interacts with M18BP1
- MCPH1 competes with M18BP1 and inhibits condensin II activity during interphase
- Phosphorylation drives a switch in binding at mitotic onset, activating condensin II

Borsellini et al., 2025, Molecular Cell *85*, 2688–2700
July 17, 2025
https://doi.org/10.1016/j.molcel.2025.06.014

CellPress

CellPress
OPEN ACCESS

Molecular Cell

Article

Condensin II activation by M18BP1

Alessandro Borsellini,[1,13] Duccio Conti,[2,13] Erin E. Cutts,[3,13,*] Rebecca J. Harris,[4,13] Kai Walstein,[2] Andrea Graziadei,[1] Valentina Cecatiello,[1] Tom F. Aarts,[4,8] Ren Xie,[5,6] Abdelghani Mazouzi,[5,6] Sushweta Sen,[4] Claire Hoencamp,[4,9] Richard Pleuger,[2,10] Sabrina Ghetti,[2] Lina Oberste-Lehn,[2] Dongqing Pan,[2,11] Tanja Bange,[2,12] Judith H.I. Haarhuis,[4] Anastassis Perrakis,[5,6] Thijn R. Brummelkamp,[5,6] Benjamin D. Rowland,[4,*] Andrea Musacchio,[2,7,*] and Alessandro Vannini[1,14,*]

[1]Human Technopole, Milan, Italy
[2]Department of Mechanistic Cell Biology, Max Planck Institute of Molecular Physiology, Dortmund, Germany
[3]School of Biosciences, Faculty of Science, University of Sheffield, Sheffield, UK
[4]Division of Cell Biology, The Netherlands Cancer Institute, Amsterdam, the Netherlands
[5]Oncode Institute, Utrecht, the Netherlands
[6]Division of Biochemistry, The Netherlands Cancer Institute, Amsterdam, the Netherlands
[7]Centre for Medical Biotechnology, Faculty of Biology, University Duisburg-Essen, Essen, Germany
[8]Present address: Department of Autonomous Matter, AMOLF, Amsterdam, the Netherlands
[9]Present address: Delft University of Technology, Delft, the Netherlands
[10]Present address: Department of Molecular Genetics, Faculty of Biology, University of Duisburg-Essen, Universitätsstrasse 5, 45117 Essen, Germany
[11]Present address: Research Division, Chugai Pharmaceutical Co., Ltd., Yokohama 244-8602, Japan
[12]Present address: Department for Systems Chronobiology, Institute of Medical Psychology, LMU Munich, Goethe-Str. 31, 80336 Munich, Germany
[13]These authors contributed equally
[14]Lead contact
*Correspondence: e.cutts@sheffield.ac.uk (E.E.C.), b.rowland@nki.nl (B.D.R.), andrea.musacchio@mpi-dortmund.mpg.de (A.M.), alessandro.vannini@fht.org (A.V.)
https://doi.org/10.1016/j.molcel.2025.06.014

SUMMARY

Condensin I and II promote the drastic spatial rearrangement of the human genome upon mitotic entry. While condensin II is known to initiate this process in early mitosis, what triggers its activation and loading onto chromatin at this juncture remains unclear. Through genetic and proteomic approaches, we identify MIS18-binding protein 1 (M18BP1), a protein required to maintain centromere identity, as the elusive factor required for condensin II localization to chromatin. M18BP1 directly binds condensin II's CAP-G2 subunit. The condensin II antagonist MCPH1 also binds to CAP-G2 and outcompetes M18BP1 during interphase to maintain the genome in its uncondensed state. A switch from MCPH1 to M18BP1 at mitotic onset activates condensin II, thus promoting proper chromosome condensation. Regulation of this M18BP1-condensin interaction thus determines both the uncondensed state of the interphase genome and its compacted state in mitosis.

INTRODUCTION

During mitosis, the eukaryotic genome must be compacted, spatially organized, and evenly dispatched to two daughter cells. Condensin complexes play a pivotal role in this process, ensuring correct chromosome segregation and genome inheritance. The two distinct condensin complexes in metazoans, condensin I and II, share their coiled-coil SMC subunits, SMC2 and SMC4, but utilize a different set of kleisin and heat-repeat-containing subunits. Condensin I contains CAP-H, CAP-D2, and CAP-G, whereas condensin II contains CAP-H2, CAP-D3, and CAP-G2 (Figure S1A).[1]

Condensin I and II exhibit distinct subcellular localization and dynamics. During interphase, condensin II is nuclear, while condensin I is mostly cytosolic and gains access to chromatin only after nuclear envelope breakdown.[2–4] Condensin II initiates chromosome condensation by shortening chromosomes, after which condensin I reduces chromosome width.[5–8] Condensin II is also enriched at kinetochores,[3,9–11] promoting chromatin assembly in the underlying centromeric regions, in turn facilitating kinetochore-microtubule attachment and errorless chromosome segregation.[12–17] As condensin II is nuclear throughout the cell cycle, it must be kept in check to limit its activation to mitotic entry. Key to this regulation is MCPH1, which prevents condensin II from stably binding to chromatin during interphase by a poorly understood mechanism. Deletion of MCPH1 results in condensin II activation and chromosome condensation during interphase.[18,19]

Here, using orthogonal approaches, we identify MIS18-binding protein 1 (M18BP1) as a determinant of condensin II localization to chromatin. In worms, this protein has been implicated in

chromosome condensation. The mechanism, however, remained unknown and was presumed to be unique to nematodes.[20] In humans, M18BP1 acts as part of the MIS18 complex during the G1 phase. This complex also comprises MIS18α and MIS18ß and associates with the histone chaperone HJURP and the kinase PLK1.[21,22] Together, these proteins ensure that the histone H3 variant CENP-A, an epigenetic marker of centromere specification, is newly deposited in early G1 to compensate for its 2-fold dilution during DNA replication.[9,15,23–30] Our data reveal that human M18BP1 has a major role that is distinct from centromere maintenance. We find that M18BP1 directly binds condensin II and that this interaction is essential to trigger chromosome condensation as cells enter mitosis. During interphase, MCPH1 keeps the genome uncondensed by counteracting M18BP1-condensin II binding. The regulation of this interaction thus determines genome architecture both in interphase and in mitosis.

RESULTS

M18BP1 interacts with condensin II

To identify new regulators of condensin II, we performed a synthetic lethality screen[31] in haploid HAP1 cells deficient for condensin I (ΔCAP-H), reasoning that they will likely be dependent on condensin II and its regulators (Figures 1A and 1B). This screen revealed that M18BP1, while not strictly essential in wild-type cells, is instead required for the fitness of cells lacking condensin I (Figure 1C).

In parallel, we performed immunoprecipitation (IP) of EGFP-M18BP1 in chromatin extracts from HeLa cells in early G1 phase and analyzed bound proteins by mass spectrometry (MS).[28] As expected, we identified all components of the MIS18 complex.[23,26,29,32–35] In addition, we identified all the subunits of condensin II but not of condensin I (Figure 1D). This is consistent with our earlier MS-based identification of M18BP1 in precipitates of an antibody against CAP-H2.[36] An essentially identical list of binding partners was identified using an mCherry-MIS18α bait (Figure S1B).

To verify the interaction happens during mitosis, we performed a coimmunoprecipitation (coIP) using EGFP-M18BP1 and confirmed by western blotting that all components of the condensin II complex co-precipitate with M18BP1 from mitotic cell lysates (Figure 1E). To assess whether M18BP1 and condensin II interact directly, we performed an *in vitro* pull-down with four MBP-tagged recombinant fragments of M18BP1 and either condensin I or condensin II (Figure 1F). The M18BP1 fragment encompassing residues 873–1,132 ($M18BP1_{873–1,132}$) was efficiently pulled down by condensin II but not condensin I (Figure 1F). Thus, $M18BP1_{873–1,132}$ binds condensin II directly, identifying M18BP1 as a condensin II interacting factor.

M18BP1 uses a short linear motif to engage CAP-G2

We next sought to map the binding site for M18BP1 on condensin II. Condensin II lacking the CAP-G2 subunit did not interact with $M18BP1_{873–1,132}$ (Figure 2A), while a subcomplex consisting of only CAP-G2 and CAP-H2 was sufficient to pull down $M18BP1_{873–1,132}$ (Figure 2A). Together this indicates that the CAP-G2 subunit is key to the M18BP1 interaction.

To further characterize the binding interface between M18BP1 and condensin II, we identified highly conserved patches within the $M18BP1_{873–1,132}$ fragment and mutated blocks of five residues (Figure S1C) to alanine. This identified M18BP1 residues 984–988 (corresponding to the motif DDHDD) as being necessary for binding (Figure S1D). In line with this, an AlphaFold-Multimer[37,38] structural model predicts with high confidence a binding interface between CAP-G2 and M18BP1 in which a partly overlapping linear motif of M18BP1 comprising residues 986–990 (HDDFF) (Figure S1E) makes extensive contacts with CAP-G2 (Figures 2B, 2C, S1F, and S1G).

To visualize the molecular interaction between M18BP1 and condensin II, we determined the cryoelectron microscopy (cryo-EM) structure of condensin II with $M18BP1_{873–1,132}$ at 7 Å average resolution, with a local resolution of 5–11 Å (Table 1). Individual subunits, generated by AlphaFold2, could be confidently assigned to the EM maps (Figures 2D, S2A–S2E, and S3A–S3C). The two SMC subunits form a parallel coiled-coil pair with the ATPase heads in close proximity, albeit not in an engaged ATP hydrolysis-competent conformation, with flexible "elbow" and "hinge" domains fading out of density. In the absence of both DNA and ATP, the overall architecture of human condensin II is reminiscent of *S. cerevisiae* condensin in its apo form,[39] but there are several unique features not observed in structures of the yeast condensin homolog, which shares more sequence homology with condensin I[39–42] (Figures S3D–S3G). CAP-D3 and CAP-G2 simultaneously bind the SMC moiety: CAP-D3 interacts with SMC2 near the ATPase head and along the coiled coil, while CAP-G2 binds SMC4 at the W-loop, in contrast to yeast condensin, where this region of SMC4 interacts with the conserved KG loop of the CAP-D3 homolog Ycs4 (Figures S3D and S3E). CAP-D3 and CAP-G2 also form a nearly continuous heat-repeat structure through interactions mediated by the "heat docker" domain of CAP-D3 (Figures 2D and S3D). The kleisin subunit, CAP-H2, binds to the heat repeats in a manner consistent with previous yeast structures and AF2 predictions, and the CAP-H2 C-terminal interface with SMC4 remains comparable to that of yeast condensin.[39–42] However, the CAP-H2 N-terminal domain, which is flexible in the yeast apo non-engaged conformation, is instead sandwiched between the SMC2 coiled-coil neck and one of the CAP-D3 heat docker helices in the human condensin II complex (Figure S3G).

An unassigned density was observed at the position where AF2 predicts the interaction between the M18BP1 "HDDFF" motif and the CAP-G2 subunit (Figure 2D). Crosslinking coupled with MS (crosslinking MS) of the condensin II-$M18BP1_{873–1,132}$ complex supports the overall architecture of the complex obtained by cryo-EM (Figures S4A–S4E). Importantly, the crosslinking data also support the interaction between M18BP1 and CAP-G2 (Figure 2E), with a specific crosslink between CAP-G2 K496 and M18BP1 L995, close to the 986-HDDFF-990 motif. We therefore mutated this motif to "HAAAA" in the $M18BP1_{873–1,132}$ fragment ($M18BP1_{4A}$) and monitored co-elution with condensin II in size-exclusion chromatography. While wild-type $M18BP1_{873–1,132}$ co-elutes with condensin II, the same fragment harboring the HAAAA mutation failed to bind and eluted in a separate peak (Figure 2F).

Next, we generated an endogenous M18BP1 mutant in HAP1 cells, with all five residues in the HDDFF motif modified to alanine

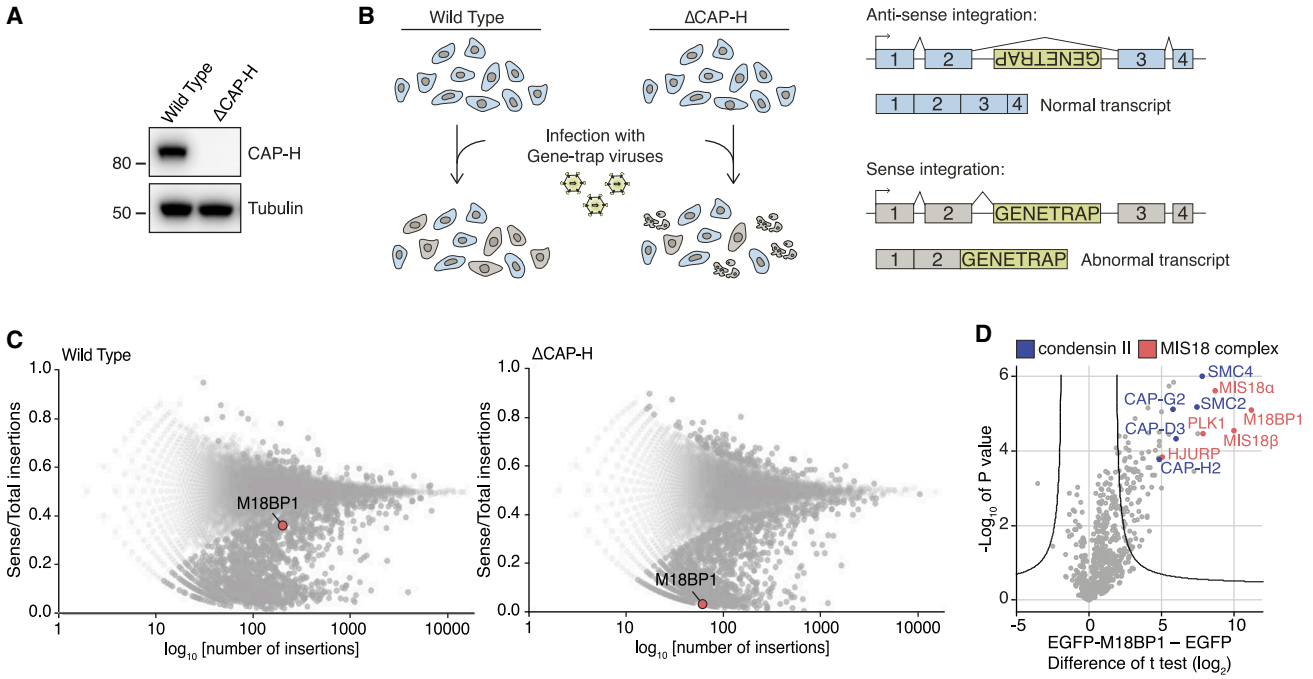

Figure 1. M18BP1 is a condensin II binding partner

(A) Western blot validating the HAP1 CAP-H knockout cell line.

(B) Schematic of the haploid genetic screening method used in (C). Cells are infected with gene-trap virus, which can integrate into gene introns in two orientations. In the antisense orientation, the integration has no effect on the gene transcript. In the sense orientation, the gene is disrupted and an abnormal transcript is produced. If a gene is essential, the population of cells with sense orientation integrations will deplete.

(C) Results of the haploid genetic screen. Each dot represents a gene, the *x* axis shows the number of gene-trap virus insertions, and the *y* axis shows the sense insertions over the total number of insertions. A value of ~0.5 indicates a non-essential gene. Lower values indicate that the gene is essential for fitness within that genetic background.

(D) Volcano plot showing the chromatin interactome of M18BP1 in early G1 phase in HeLa cells. Condensin II subunits are marked in blue, whereas the CENP-A deposition machinery components are marked in red.

(E) Chromatin-bound EGFP-M18BP1 co-immunoprecipitates condensin II in mitotic HeLa cells.

(F) *In vitro* pull-down using indicated fragments of MBP-tagged M18BP1 with human condensin I or II. Asterisk indicates the pulled-down M18BP1 fragment.

($M18BP1_{5A}$). We also endogenously tagged the condensin II subunit CAP-H2 with Halo-3xHA in both wild-type and M18BP1 mutant cells (Figure S4F). Immunoprecipitated CAP-H2-Halo-3xHA pulled down wild-type M18BP1 but not $M18BP1_{5A}$ (Figure 2G). Taken together, these results indicate that M18BP1 and condensin II form a stable complex that is mediated, partly or entirely, by an interaction between a conserved M18BP1 linear motif and the condensin II subunit CAP-G2.

M18BP1's HDDFF motif localizes condensin II to chromatin

We then investigated the role of M18BP1 binding to condensin II. As expected, in the wild-type HAP1 cells, CAP-H2 was highly enriched on chromatin during mitosis. Remarkably, in $M18BP1_{5A}$ cells, CAP-H2 was almost undetectable on chromosomes (Figures 3A and 3B). This observation was corroborated by imaging untagged CAP-D3 in HeLa cells expressing small interfering RNA (siRNA)-resistant, mCherry-tagged wild-type M18BP1 or

CellPress
OPEN ACCESS

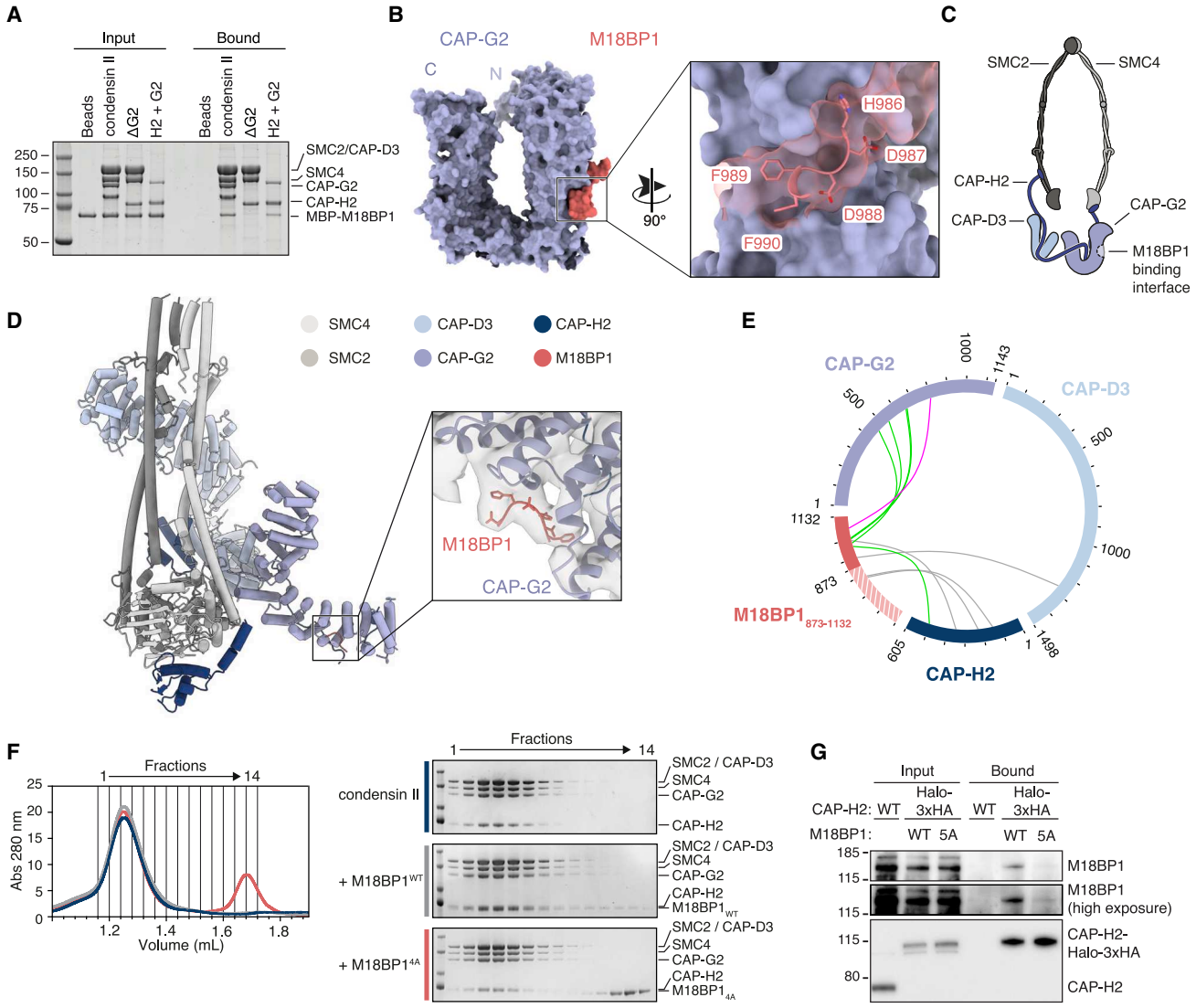

Figure 2. M18BP1 binds to the condensin II CAP-G2 subunit

(A) Pull down of condensin II (CAP-H2 strep tag) in the presence of MBP-M18BP1$_{873–1,132}$. The full-length condensin II complex, the complex missing CAP-G2 (ΔG2), or only the CAP-H2 and CAP-G2 subunits were used. In the latter two, the strep tag was cleaved from CAP-H2.

(B) AF2 multimer prediction of CAP-G2 (purple) with M18BP1 (red), with a zoom-in of the "HDDFF" motif of M18BP1.

(C) Cartoon representation of the condensin II complex.

(D) Cryo-EM structure of apo condensin II holo-complex displaying SMC subunits in gray, CAP-D3 in light blue, CAP-G2 in purple, and CAP-H2 in dark blue and a zoom-in of the extra density at the CAP-G2-M18BP1 (red) interaction interface.

(E) Intermolecular sulfo-SDA crosslinks between M18BP1$_{873–1,132}$ and condensin II subunits.

(F) Size-exclusion profiles of condensin II (blue), condensin II with M18BP1$_{WT-873–1,132}$ (gray), and condensin II with M18BP1$_{4A-873–1,132}$ (red). Fractions from size-exclusion profiles are shown in the SDS-PAGE gels in the lower panels.

(G) Western blot analysis after coIP using anti-HA beads in wild-type (WT) HAP1 cells expressing endogenous untagged CAP-H2 (control cells), WT cells expressing endogenously tagged CAP-H2-Halo-3xHA, or M18BP1$_{5A}$ (HDDFF mutant) cells expressing CAP-H2-Halo-3xHA.

M18BP1$_{4A}$ mutant. CAP-D3 was no longer detected on metaphase chromosomes depleted of M18BP1 by RNAi (Figures S5A–S5C). Ectopic expression of wild-type M18BP1 rescued CAP-D3 localization to mitotic chromosomes, whereas expression of M18BP1$_{4A}$ failed to do so (Figures S5A, S5B, S5D, and S5E). We also directly compared the M18BP1 4A and 5A mutants by generating M18BP1$_{4A}$ HAP1 cells. As expected, CAP-H2 levels on chromatin were undetectable, as in the M18BP1$_{5A}$ mutant (Figures S4F and S5F). The depletion of M18BP1 prior to mitotic entry did not affect the overall levels or nuclear localization of CAP-D3 in G2 cells (Figures S5G–S5K). Together, these results show that M18BP1 plays a central role in condensin II association with chromatin during mitosis and that this role requires the M18BP1 HDDFF motif.

Table 1. Cryo-EM data collection, refinement, and validation statistics

Data collection and processing	Condensin II-M18BP1
Magnification	105,000
Voltage (kV)	300
Electron exposure $e^{-}/Å^2$	50
Defocus range (μm)	0.8–2.0
Pixel size (Å)	1.2
Symmetry imposed	C1
Initial particle images (no)	3.7 M
Final particle images (no)	49,000
Map resolution (Å)	7
FSC threshold	1.43
Map resolution range (Å)	5 to ∼11
Refinement	
Initial model used	Alphafold monomer predictions
Model resolution (Å)	6.6
FSC threshold	0.143
Map sharpening B factor ($Å^2$)	−300
Model comparison	
Nonhydrogen atoms	23,364
Protein residues	2,891
RMSDs	
Bond lengths ($Å^2$)	0.005
Bond angles (°)	1.043
Validation	
MolProbity score	1.64
Clashscore	8.27
Poor rotamers (%)	1.77
Ramachandran plot	
Favored (%)	96.85
Allowed (%)	3.12
Outliers (%)	0.04

As M18BP1 mutant cells have no detectable condensin II on mitotic chromosomes (Figures 3A and S5A–S5E), we used chromosome spreads to determine whether these cells display condensation defects. As expected, wild-type cells showed condensed mitotic chromosomes, whereas cells lacking functional condensin II (ΔCAP-H2 cells) showed poorly condensed chromosomes. M18BP1$_{5A}$ cells displayed condensation defects as pervasive as those observed in the absence of CAP-H2 (Figures 3C and 3D) but—for unclear reasons—with a different distribution of aberrant chromosome morphologies. We tested whether these differences could be explained by changes in condensin I levels on the chromatin during mitosis, but chromatin fractionation showed normal condensin I levels in M18BP1 mutant cells (Figure S6A). Consistent with the condensation defects detected in M18BP1$_{5A}$ chromosome spreads, inter-kinetochore distances on condensed chromosomes under microtubule-generated tension were significantly longer in cells depleted of M18BP1 relative to non-depleted controls and phenocopied the loss of condensin II (Figures S6A–S6D). Together, these results corroborate the idea that M18BP1 is required for condensin II-mediated chromosome condensation.

Since M18BP1 is essential for the deposition of the centromeric marker CENP-A,[23,28,30,43] we asked whether disruption of the HDDFF motif also affects this pathway. Labeling of newly deposited CENP-A showed that M18BP1$_{4A}$ is as efficient in depositing CENP-A as wild-type M18BP1 (Figures 3E and S6E–S6G). Thus, mutating the M18BP1 HDDFF motif yields a separation-of-function mutant that ablates condensin II localization to mitotic chromosomes but does not affect CENP-A deposition.

M18BP1 enhances condensin II DNA-dependent ATPase activity

Condensin II-mediated chromosome condensation is dependent on its ATPase activity.[44,45] We therefore asked whether M18BP1 might affect condensin II ATPase activity. In line with previous evidence,[46] DNA stimulated the ATP hydrolysis rate of condensin II by ∼2.5-fold, and the addition of M18BP1$_{873–1,132}$ further stimulated the ATP hydrolysis rate, but the effect was less pronounced if DNA was omitted (Figure 3F). The M18BP1$_{4A}$ mutant did not enhance condensin II ATPase activity, indicating that a direct interaction between M18BP1 and condensin II is required to stimulate ATP hydrolysis. A hydrolysis-deficient condensin II mutant—SMC2 Q147L and SMC4 Q229L[47]—did not display ATPase activity, even upon addition of DNA or M18BP1 (Figure 3F).

M18BP1 competes with the condensin II antagonist MCPH1

MCPH1 binds the CAP-G2 subunit of condensin II using a conserved "central domain."[18,19] We noted that a highly conserved "YDDYF" motif within the MCPH1 central domain is remarkably similar to the HDDFF motif of M18BP1 (Figure 4A), thus suggesting that MCPH1 and M18BP1 may compete for the same interface of condensin II. Confirming this idea, AF2 predicts with high confidence that the YDDYF of MCPH1 and the HDDFF motif of M18BP1 bind the same interface of CAP-G2 (Figures 4B and S7A). Crosslinking MS of condensin II in complex with MCPH1$_{1–435}$ identified multiple crosslinks connecting the MCPH1 central domain to the predicted interface of CAP-G2 (Figure 4C). We then used fluorescence anisotropy competition assays to assess whether MCPH1 and M18BP1 compete for condensin II binding. Using an MCPH1$_{407–424}$ 5-FAM-labeled peptide with a fixed concentration of condensin II and increasing concentrations of unlabeled M18BP1 or MCPH1, we confirmed that M18BP1 and MCPH1 compete for condensin II binding (Figure 4D).

MCPH1 prevents interphase condensation by counteracting M18BP1

Although our biochemical observations identify M18BP1 and MCPH1 as competitive partners of condensin II *in vitro*, whether competition occurs *in vivo* is unclear. To address this question, we first assessed the localization of M18BP1 during the cell cycle. In both HeLa and RPE1 cells, M18BP1 was strongly enriched at centromeres during early G1 phase, as observed previously[23] (Figures S7B–S7G). We also observed substantial levels of

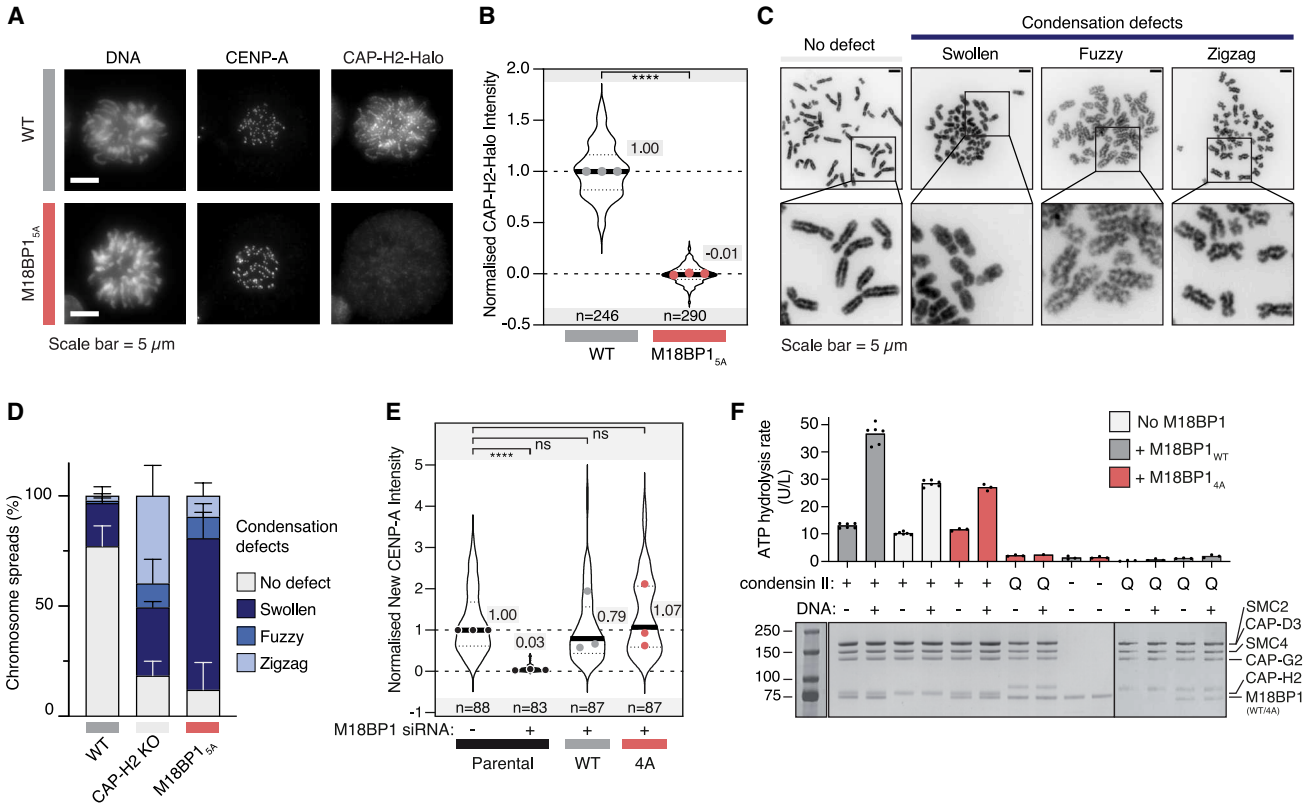

Figure 3. M18BP1 is a major recruiter of condensin II during mitosis

(A) Representative images of endogenously tagged CAP-H2-Halo-3xHA levels on mitotic chromatin in WT or M18BP1$_{5A}$ "HDDFF" mutant HAP1 cells.

(B) Quantification of CAP-H2-Halo-3xHA levels from (A). "*n*" represents the total number of cells from three independent experiments. The median of the combined data is shown for each condition, and dots show the median of each experimental repeat.

(C) Example images of mitotic chromosome spreads with condensation defects as quantified in (D).

(D) The percentage of chromosome spreads with condensation defects in WT, ΔCAP-H2, and M18BP1$_{5A}$ cells. Bars represent mean ± SD.

(E) The M18BP1$_{4A}$ mutant does not affect new CENP-A deposition. Plot shows the intensity of the newly deposited CENP-A in the indicated conditions in HeLa cells. n represents the total number of cells from three independent experiments. The median of the combined data is shown for each condition, and dots show the median of each experimental repeat.

(F) ATPase rate of the condensin II complex in the presence of M18BP1$_{873–1,132}$ and DNA. Q refers to condensin II with an ATPase-deficient mutation in the Q-loop. 4A refers to the M18BP1$_{4A}$ mutant. Below is an SDS-PAGE gel showing the loading controls. Black dots are individual values from 3 to 6 independent experiments.

M18BP1 in S phase and G2 at both the centromeres and throughout the nucleus (Figures S7B–S7G). Thus, M18BP1 localizes to chromatin well before mitotic onset, suggesting that there could be competition between MCPH1 and M18BP1 for condensin II binding. Nonetheless, condensin II does not associate stably with chromatin until the onset of mitosis.

In cells lacking MCPH1, condensin II stably binds to chromatin during interphase, resulting in interphase chromosome condensation.[19] At least two mutually exclusive scenarios may underlie this interphase condensation. In the first scenario, condensin II is sufficient for autonomous localization to chromatin, and M18BP1 is merely required to relieve repression by MCPH1 as cells enter mitosis. In the second scenario, condensin II requires M18BP1 to localize to chromatin, and MCPH1 prevents M18BP1 from acting during interphase, limiting condensin II activity to mitosis. To distinguish between these two possibilities, we utilized the interphase condensation phenotype observed in MCPH1-deficient cells. As expected, chromosome condensation was observed in G2 cells upon depletion of MCPH1 (Figures 4E, 4F, and S7H). Importantly, condensation was completely suppressed when M18BP1 was also depleted (Figures 4E–4G), even when cells progressed into mitosis (Figures S7I and S7J). Thus, M18BP1 is required for condensin II-mediated chromosome condensation in cells lacking MCPH1. This suggests that M18BP1 does not merely interact with condensin II to counteract MCPH1. Instead, our data support a scenario in which M18BP1 plays a central role in condensin II's ability to condense chromatin and in which MCPH1 prevents interphase condensation by counteracting M18BP1.

Phosphorylation triggers a switch from MCPH1 to M18BP1

Both MCPH1 and M18BP1 harbor consensus sites for the mitotic kinase CDK1 adjacent to the CAP-G2 binding motif (Figure S8A). In MCPH1, phosphorylation at S417 hinders its binding to CAP-G2 (Figure S8B), consistent with previous

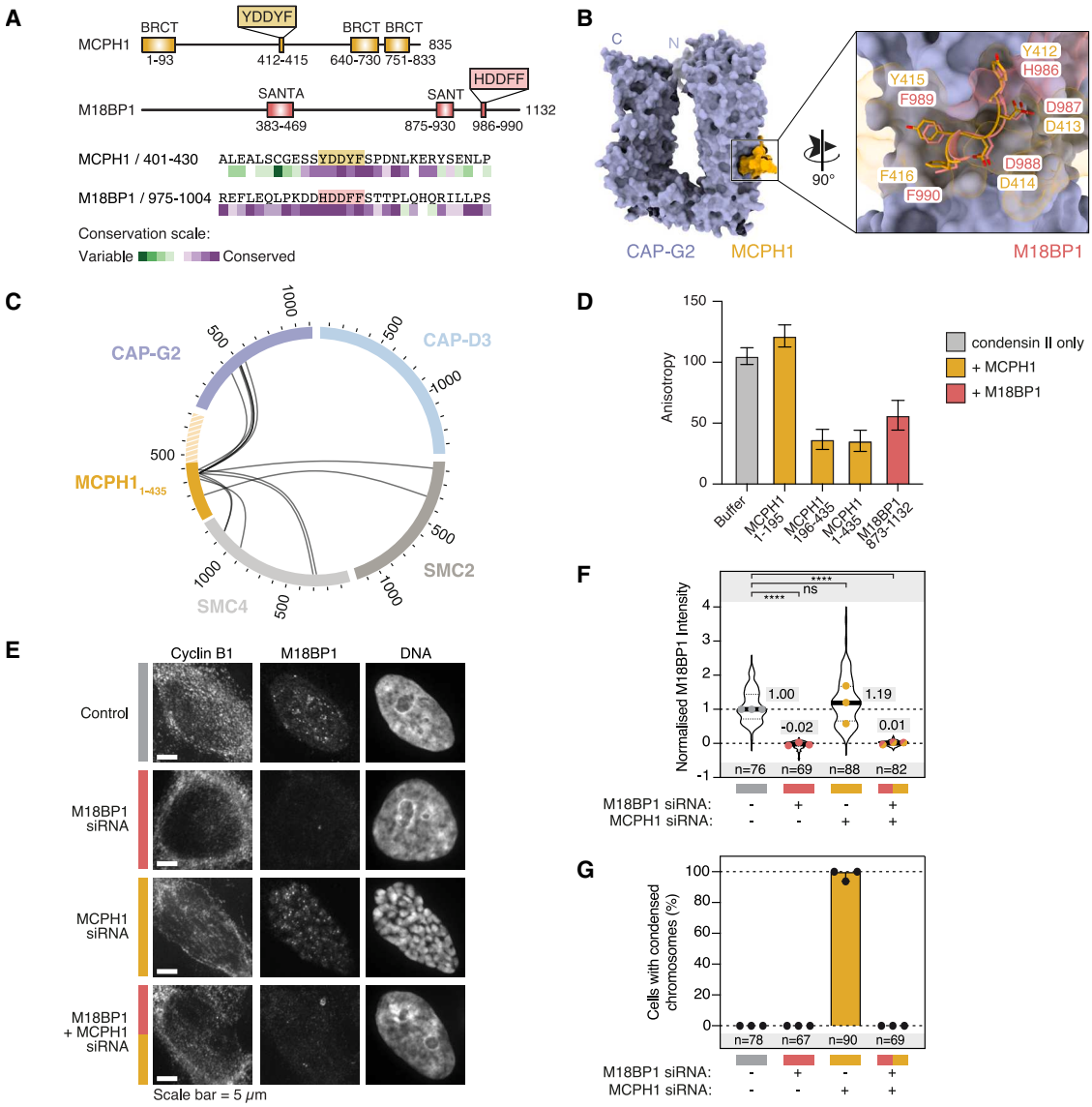

Figure 4. MCPH1-M18BP1 competition keeps the interphase genome uncondensed

(A) Schematic of M18BP1 and MCPH1 indicating the identified binding motifs. Below shows the alignment of the motifs colored by conservation score from ConSurf.

(B) AF2 multimer structural prediction of CAP-G2 bound to MCPH1 and M18BP1. The two predictions were overlaid using CAP-G2 as the reference. For clarity, only the YDDYF/HDDFF motifs are shown.

(C) Crosslinking MS of MCPH1$_{1–435}$ bound to condensin II.

(D) Fluorescence anisotropy competition assay using a 5-FAM-MCPH1$_{407–424}$ peptide probe at 0.3 and 0.8 μM condensin II, with indicated MCPH1 or M18BP1 fragments added to compete with the probe. Mean and standard error from n = 3 repeats.

(E) Example images of the chromosome condensation status of HeLa cells in G2 when treated with different combinations of siRNA.

(F) Quantification of M18BP1 chromatin levels from (E). "n" represents the number of cells analyzed across three independent experimental repeats. The median of the combined data is shown for each condition, and dots show the median of each experimental repeat.

(G) Quantification of the chromosome condensation status of cells from (E). Bars and whiskers indicate the median and 95% confidence interval, respectively.

work.[19] By contrast, studies in *C. elegans* suggest that CDK1 phosphorylation of the M18BP1 ortholog KLN-2 is necessary for condensin II recruitment to mitotic chromosomes.[20] Importantly, deposited datasets of the human phosphoproteome[48] as well as the crosslinking MS dataset reported here identify multiple phosphorylation sites on M18BP1 near the HDDFF motif (Tables S2 and S3).

We therefore hypothesized that phosphorylation of M18BP1 may increase its affinity for condensin II. To test this hypothesis, we performed fluorescence anisotropy competition assays in which M18BP1 was titrated against a fixed concentration of condensin II and a 5-FAM-MCPH1$_{407–424}$ peptide. We used an M18BP1 fragment (residues 983–1,045) harboring the wild-type sequence, as well as a mutant version in which seven potential

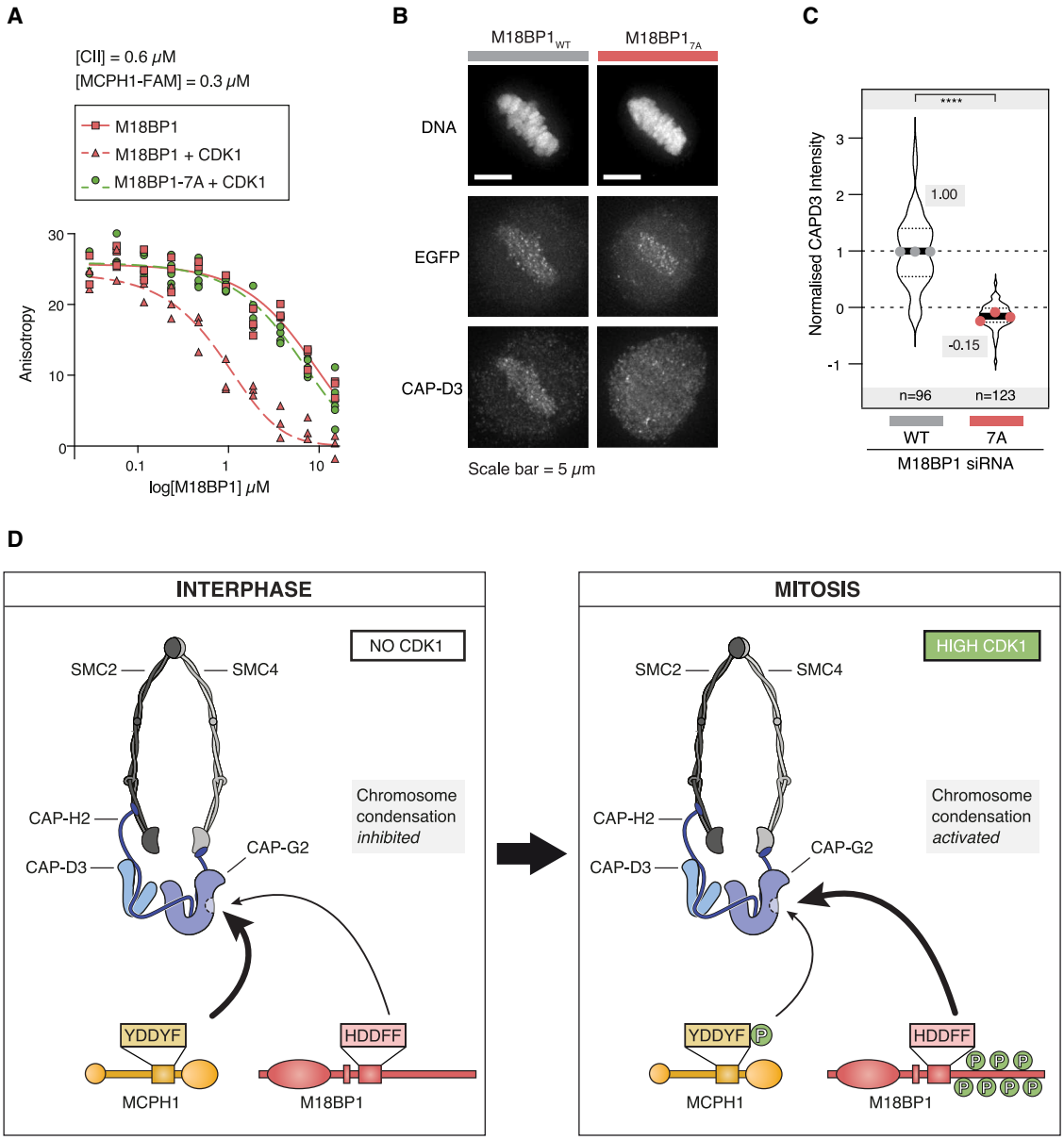

Figure 5. A model for condensin II activation

(A) Fluorescence anisotropy competition assay using a 5-FAM-MCPH1$_{407–424}$ peptide and condensin II at a fixed concentration (0.3 and 0.6 μM, respectively), with increasing concentrations of M18BP1$_{983–1,045\text{-WT}}$ or M18BP1$_{983–1,045\text{-7A}}$ with or without CDK1-cyclin B treatment.

(B) Example images of CAP-D3 localization on chromosomes in HeLa cells conditionally expressing siRNA-resistant mCherry-M18BP1 WT or 7A mutant.

(C) Quantification of endogenous CAP-D3 from (B). "*n*" represents the total number of cells from three independent experiments. The median of the combined data is shown for each condition, and dots show the median of each experimental repeat.

(D) During interphase (left), MCPH1 binds to CAP-G2 and inhibits condensin II activity. Upon mitotic entry (right), high CDK1 activity induces phosphorylation of both MCPH1 and M18BP1. This leads to a switch from MCPH1 to M18BP1 binding to CAP-G2, thus activating condensin II and initiating chromosome condensation.

phosphorylation sites (S/T) are replaced by alanines (M18BP1$_{7A}$) (Table S2). CDK1-cyclin B treatment resulted in phosphorylation of the wild-type M18BP1 peptide but not the 7A mutant (Figure S8C). The unphosphorylated wild-type M18BP1$_{983–1,045}$ competes with FAM-MCPH1$_{407–424}$, with a K_{D2} of 20.0 ± 4.9 μM. The phosphorylated wild-type M18BP1$_{983–1,045}$ more readily competes, yielding a K_{D2} of 0.7 ± 0.4 μM. The M18BP1$_{983–1,045}$-7A mutant, however, remained unaffected by CDK1-cyclin B treatment, with a K_{D2} of 15.6 ± 5 μM, similar to that of the unphosphorylated wild type (Figure 5A). Phosphorylation therefore enhances the ability of M18BP1 to outcompete MCPH1 for condensin II binding.

To assess the role of M18BP1 phosphorylation *in vivo*, we imaged endogenous CAP-D3 in HeLa cells expressing an

siRNA-resistant EGFP-tagged wild-type M18BP1 or the M18BP1$_{7A}$ mutant. CAP-D3 was no longer detected on metaphase chromosomes depleted of M18BP1 by RNAi (Figures S8D–S8F). Consistent with the biochemical observations, ectopic expression of wild-type M18BP1 rescued CAP-D3 localization to mitotic chromosomes, whereas expression of M18BP1$_{7A}$ failed to do so (Figures 5B, 5C, and S8G).

Together, these data show a phosphorylation-driven switch between MCPH1 and M18BP1 binding to CAP-G2, thus allowing precise temporal regulation of condensin II activity at the onset of mitosis (Figure 5C).

DISCUSSION

M18BP1 is well-known for its role in maintaining centromere-specific chromatin through the deposition of CENP-A during G1.[9,25] Here, we identify M18BP1 as a crucial regulator of chromosome condensation. We show that an M18BP1 mutant impaired in condensin II binding retains the ability to load new CENP-A, highlighting a moonlighting function for M18BP1 in chromosome condensation. Collectively, our observations argue that during interphase MCPH1 counteracts condensin II activation by M18BP1 by directly competing for binding to CAP-G2 and preventing the stable association of condensin II with chromatin (Figure 5C). This maintains the interphase genome in its uncompacted state. At the onset of mitosis, both M18BP1 and MCPH1 are phosphorylated, likely by CDK1. This switches binding preferences, now favoring M18BP1 over MCPH1, resulting in condensin II localization to chromatin and chromosome condensation specifically as cells enter mitosis (Figure 5C). Mutations in MCPH1 cause premature chromosome condensation syndrome,[49] which is a clinical phenotype associated with microcephaly.[50] The data presented here demonstrate that premature chromosome condensation, caused by loss of MCPH1, requires M18BP1-dependent activation of condensin II. Such unrestricted M18BP1-mediated condensin II activation may therefore contribute to this disease.

The structural data presented here offer insights into the regulation of condensin II and its activation by M18BP1. The cryo-EM structure of condensin II with M18BP1 reveals an interaction between CAP-D3 and CAP-G2, mediated by the CAP-D3 heat docker domain. The interaction between CAP-D3 and CAP-G2 has been associated with a self-repressed conformation that inhibits condensin II activity in *Xenopus* egg extracts.[51] This seemingly contrasts with the role of M18BP1 as an activator of condensin II, raising the possibility that additional factors such as ATP binding or DNA engagement are required to further rearrange condensin II. This idea is supported by structural comparisons with other SMC complexes (Figure S3F), where DNA and ATP binding causes significant rearrangements of the heat repeats and SMC coiled coils.[42,52,53]

Our data combined with previous results highlight how phosphorylation plays a pivotal role in condensin II regulation. Phosphorylation of the CAP-D3 C-terminal tail by CDK1 is implicated in activating condensin II by releasing its self-repressed interaction with CAP-G2.[51] Simultaneously, M18BP1 phosphorylation enhances its ability to compete with MCPH1 for condensin II binding, suggesting a complementary layer of regulation. CDK1-mediated phosphorylation of KNL-2, the *C. elegans* homolog of M18BP1, is important for mitotic chromosome condensation in nematodes.[20] As the KNL-2 phosphorylation sites are not conserved between nematodes and vertebrates, the role of KNL-2 in chromosome condensation was proposed to be nematode-specific. Our finding of a direct association between M18BP1 and condensin II and of its potential regulation by CDK1, however, argues for a conserved mechanism that exploits a single protein for multiple independent functions—centromere maintenance and condensin II regulation.

The competition between M18BP1 and MCPH1 occurs through similar linear motifs that bind to a common pocket in the CAP-G2 subunit. Interestingly, an analogous regulatory mechanism has been proposed for the cohesin complex, in which regulatory factors compete for a common binding pocket to allow cohesin to either build loops or hold together the sister chromatids.[54,55] This binding pocket on cohesin is within the SA1/SA2 subunit, which is paralogous to CAP-G2. Similarly, yeast condensin and human condensin I may also have such "binding hubs."[56,57] Thus, distinct but related SMC complexes may deploy similar mechanisms to regulate their activity. Collectively, these data suggest a conserved principle of regulation that allows these molecular machines to shape the genome and thereby enable crucial genomic events.

Limitations of the study

This study highlights the opposing roles of MCPH1 and M18BP1 in regulating condensin II. Both MCPH1 and M18BP1 bind to the CAP-G2 subunit of condensin II using a short linear motif, but the molecular mechanism by which M18BP1 activates condensin II remains unclear.

RESOURCE AVAILABILITY

Lead contact

Further information and requests for resources should be directed to the lead contact, Alessandro Vannini (alessandro.vannini@fht.org).

Materials availability

Requests for generated materials should be directed to the corresponding authors.

Data and code availability

- The cryo-EM map of the condensin II-M18BP1 complex has been deposited in the Electron Microscopy Data Bank (EMDB) with accession code EMD-50201. The atomic coordinates of the condensin II-M18BP1 complex have been deposited in the Protein Data Bank (PDB) with accession code 9F5W.
- The MS proteomics data have been deposited to the ProteomeXchange Consortium (http://proteomecentral.proteomexchange.org) via the PRIDE partner repository with the dataset identifier PXD051556.
- The MS crosslinking MS data for condensin II-M18BP1 have been deposited to the ProteomeXchange Consortium (http://proteomecentral.proteomexchange.org) via the PRIDE partner repository with the dataset identifier PXD051886 and 10.6019/PXD051886.
- The genetic screen dataset has been deposited to the European Nucleotide Archive with accession number PRJEB89880.
- This paper does not report original code.
- Any additional information required to reanalyze the data reported in this paper is available from the lead contact upon request.

ACKNOWLEDGMENTS

We thank Martin Houlard for helpful discussions regarding MCPH1 and Norman Davey for helpful discussions on short linear motifs. We thank P. Swuec and S. Sorrentino of the Cryo-Electron Microscopy Unit of the National Facility for Structural Biology at Human Technopole for technical support and assistance. This work was supported by the Max Planck Society (A. Musacchio). European Research Council Synergy Grant 951430 BIOMECANET (A. Musacchio), DGF's Collaborative Research Centre 1430 "Molecular Mechanisms of Cell State Transitions" (A. Musacchio), CANTAR network under the Netzwerke-NRW programme (A. Musacchio), Human Technopole MEF (A.V.), Cancer Research UK Programme Foundation CR-UK C47547/A21536 (A.V.), Wellcome Trust Investigator Award 200818/Z/16/Z (A.V.), Dutch Research Council (NWO, VI.C.202.098 to B.D.R.), Dutch Cancer Society (12687 to B.D.R. and 15868 to B.D.R. and R.J.H.), EMBO Long-Term Fellowship ALTF 439-2019 (D.C.), and EMBO Long-Term Fellowship ALTF 552-2022 (A.B.).

AUTHOR CONTRIBUTIONS

A.B., D.C., E.E.C., R.J.H., B.D.R., A. Musacchio, and A.V. conceived the experiments. A.B., D.P., and E.E.C. performed *in vitro* experiments. A.B. performed cryo-EM experiments. R.J.H. performed all HAP1 cell biology experiments with the exception of the haploid genetic screen. D.C., R.P., S.G., and L.O.-L. performed cell biology experiments in HeLa and RPE1 cells. R.J.H., T.F.A., and C.H. generated endogenously mutated HAP1 cell lines. D.C., S.G., and L.O.-L. generated the HeLa Flp-In T-REx cell lines and the endogenously tagged RPE1 cell lines. S.S. and J.H.I.H. performed and A. Mazouzi analyzed, haploid genetic screens. K.W. and T.B. performed the coIP MS analysis. A.B., E.E.C., R.J.H., and R.X. generated and analyzed AlphaFold models. A.B., A.G., and V.C. prepared samples for crosslinking (XL)-MS experiments. A.G. collected and analyzed XL-MS data. A.B., D.C., E.E.C., R.J.H., B.D.R., A. Musacchio, and A.V. wrote the manuscript with input from all authors. D.C., R.J.H., J.H.I.H., A.P., T.R.B., B.D.R., A. Musacchio, and A.V. provided supervision. A.B., D.C., R.J.H., B.D.R., A. Musacchio, and A.V. acquired funding.

DECLARATION OF INTERESTS

The authors declare no competing interests.

STAR★METHODS

Detailed methods are provided in the online version of this paper and include the following:

SUPPLEMENTAL INFORMATION

Supplemental information can be found online at https://doi.org/10.1016/j.molcel.2025.06.014.

Received: May 6, 2024
Revised: March 25, 2025
Accepted: June 16, 2025
Published: July 3, 2025

REFERENCES

1. Hoencamp, C., and Rowland, B.D. (2023). Genome control by SMC complexes. Nat. Rev. Mol. Cell Biol. *24*, 633–650. https://doi.org/10.1038/s41580-023-00609-8.
2. Hirota, T., Gerlich, D., Koch, B., Ellenberg, J., and Peters, J.M. (2004). Distinct functions of condensin I and II in mitotic chromosome assembly. J. Cell Sci. *117*, 6435–6445. https://doi.org/10.1242/jcs.01604.
3. Ono, T., Fang, Y., Spector, D.L., and Hirano, T. (2004). Spatial and temporal regulation of Condensins I and II in mitotic chromosome assembly in human cells. Mol. Biol. Cell *15*, 3296–3308. https://doi.org/10.1091/mbc.e04-03-0242.
4. Ono, T., Losada, A., Hirano, M., Myers, M.P., Neuwald, A.F., and Hirano, T. (2003). Differential contributions of condensin I and condensin II to mitotic chromosome architecture in vertebrate cells. Cell *115*, 109–121. https://doi.org/10.1016/s0092-8674(03)00724-4.
5. Green, L.C., Kalitsis, P., Chang, T.M., Cipetic, M., Kim, J.H., Marshall, O., Turnbull, L., Whitchurch, C.B., Vagnarelli, P., Samejima, K., et al. (2012). Contrasting roles of condensin I and condensin II in mitotic chromosome formation. J. Cell Sci. *125*, 1591–1604. https://doi.org/10.1242/jcs.097790.
6. Shintomi, K., and Hirano, T. (2011). The relative ratio of condensin I to II determines chromosome shapes. Genes Dev. *25*, 1464–1469. https://doi.org/10.1101/gad.2060311.
7. Gibcus, J.H., Samejima, K., Goloborodko, A., Samejima, I., Naumova, N., Nuebler, J., Kanemaki, M.T., Xie, L., Paulson, J.R., Earnshaw, W.C., et al. (2018). A pathway for mitotic chromosome formation. Science *359*, eaao6135. https://doi.org/10.1126/science.aao6135.
8. Walther, N., Hossain, M.J., Politi, A.Z., Koch, B., Kueblbeck, M., Ødegård-Fougner, Ø., Lampe, M., and Ellenberg, J. (2018). A quantitative map of human Condensins provides new insights into mitotic chromosome architecture. J. Cell Biol. *217*, 2309–2328. https://doi.org/10.1083/jcb.201801048.
9. Foltz, D.R., Jansen, L.E.T., Bailey, A.O., Yates, J.R., 3rd, Bassett, E.A., Wood, S., Black, B.E., and Cleveland, D.W. (2009). Centromere-specific assembly of CENP-a nucleosomes is mediated by HJURP. Cell *137*, 472–484. https://doi.org/10.1016/j.cell.2009.02.039.
10. Tada, K., Susumu, H., Sakuno, T., and Watanabe, Y. (2011). Condensin association with histone H2A shapes mitotic chromosomes. Nature *474*, 477–483. https://doi.org/10.1038/nature10179.
11. Ohta, S., Montaño-Gutierrez, L.F., de Lima Alves, F., Ogawa, H., Toramoto, I., Sato, N., Morrison, C.G., Takeda, S., Hudson, D.F., Rappsilber, J., et al. (2016). Proteomics Analysis with a Nano Random Forest Approach Reveals Novel Functional Interactions Regulated by

SMC Complexes on Mitotic Chromosomes. Mol. Cell. Proteomics *15*, 2802–2818. https://doi.org/10.1074/mcp.M116.057885.

12. Kim, J.H., Shim, J., Ji, M.J., Jung, Y., Bong, S.M., Jang, Y.J., Yoon, E.K., Lee, S.J., Kim, K.G., Kim, Y.H., et al. (2014). The condensin component NCAPG2 regulates microtubule-kinetochore attachment through recruitment of Polo-like kinase 1 to kinetochores. Nat. Commun. *5*, 4588. https://doi.org/10.1038/ncomms5588.
13. Bernad, R., Sánchez, P., Rivera, T., Rodríguez-Corsino, M., Boyarchuk, E., Vassias, I., Ray-Gallet, D., Arnaoutov, A., Dasso, M., Almouzni, G., et al. (2011). Xenopus HJURP and condensin II are required for CENP-A assembly. J. Cell Biol. *192*, 569–582. https://doi.org/10.1083/jcb.201005136.
14. Samoshkin, A., Arnaoutov, A., Jansen, L.E.T., Ouspenski, I., Dye, L., Karpova, T., McNally, J., Dasso, M., Cleveland, D.W., and Strunnikov, A. (2009). Human condensin function is essential for centromeric chromatin assembly and proper sister kinetochore orientation. PLOS One *4*, e6831. https://doi.org/10.1371/journal.pone.0006831.
15. Barnhart-Dailey, M.C., Trivedi, P., Stukenberg, P.T., and Foltz, D.R. (2017). HJURP interaction with the condensin II complex during G1 promotes CENP-A deposition. Mol. Biol. Cell *28*, 54–64. https://doi.org/10.1091/mbc.E15-12-0843.
16. Hudson, D.F., Vagnarelli, P., Gassmann, R., and Earnshaw, W.C. (2003). Condensin is required for nonhistone protein assembly and structural integrity of vertebrate mitotic chromosomes. Dev. Cell *5*, 323–336. https://doi.org/10.1016/s1534-5807(03)00199-0.
17. Ribeiro, S.A., Gatlin, J.C., Dong, Y., Joglekar, A., Cameron, L., Hudson, D. F., Farr, C.J., McEwen, B.F., Salmon, E.D., Earnshaw, W.C., et al. (2009). Condensin regulates the stiffness of vertebrate centromeres. Mol. Biol. Cell *20*, 2371–2380. https://doi.org/10.1091/mbc.e08-11-1127.
18. Yamashita, D., Shintomi, K., Ono, T., Gavvovidis, I., Schindler, D., Neitzel, H., Trimborn, M., and Hirano, T. (2011). MCPH1 regulates chromosome condensation and shaping as a composite modulator of condensin II. J. Cell Biol. *194*, 841–854. https://doi.org/10.1083/jcb.201106141.
19. Houlard, M., Cutts, E.E., Shamim, M.S., Godwin, J., Weisz, D., Presser Aiden, A., Lieberman Aiden, E., Schermelleh, L., Vannini, A., and Nasmyth, K. (2021). MCPH1 inhibits Condensin II during interphase by regulating its SMC2-Kleisin interface. eLife *10*, e73348. https://doi.org/10.7554/eLife.73348.
20. Wenda, J.M., Prosée, R.F., Gabus, C., and Steiner, F.A. (2021). Mitotic chromosome condensation requires phosphorylation of the centromeric protein KNL-2 in C. elegans. J. Cell Sci. *134*, jcs259088. https://doi.org/10.1242/jcs.259088.
21. Sundararajan, K., and Straight, A.F. (2022). Centromere Identity and the Regulation of Chromosome Segregation. Front. Cell Dev. Biol. *10*, 914249. https://doi.org/10.3389/fcell.2022.914249.
22. Stellfox, M.E., Bailey, A.O., and Foltz, D.R. (2013). Putting CENP-A in its place. Cell. Mol. Life Sci. *70*, 387–406. https://doi.org/10.1007/s00018-012-1048-8.
23. Fujita, Y., Hayashi, T., Kiyomitsu, T., Toyoda, Y., Kokubu, A., Obuse, C., and Yanagida, M. (2007). Priming of centromere for CENP-A recruitment by human hMis18alpha, hMis18beta, and M18BP1. Dev. Cell *12*, 17–30. https://doi.org/10.1016/j.devcel.2006.11.002.
24. Jansen, L.E.T., Black, B.E., Foltz, D.R., and Cleveland, D.W. (2007). Propagation of centromeric chromatin requires exit from mitosis. J. Cell Biol. *176*, 795–805. https://doi.org/10.1083/jcb.200701066.
25. Dunleavy, E.M., Roche, D., Tagami, H., Lacoste, N., Ray-Gallet, D., Nakamura, Y., Daigo, Y., Nakatani, Y., and Almouzni-Pettinotti, G. (2009). HJURP is a cell-cycle-dependent maintenance and deposition factor of CENP-A at centromeres. Cell *137*, 485–497. https://doi.org/10.1016/j.cell.2009.02.040.
26. Spiller, F., Medina-Pritchard, B., Abad, M.A., Wear, M.A., Molina, O., Earnshaw, W.C., and Jeyaprakash, A.A. (2017). Molecular basis for Cdk1-regulated timing of Mis18 complex assembly and CENP-A deposition. EMBO Rep. *18*, 894–905. https://doi.org/10.15252/embr.201643564.
27. Pan, D., Walstein, K., Take, A., Bier, D., Kaiser, N., and Musacchio, A. (2019). Mechanism of centromere recruitment of the CENP-A chaperone HJURP and its implications for centromere licensing. Nat. Commun. *10*, 4046. https://doi.org/10.1038/s41467-019-12019-6.
28. Pan, D., Klare, K., Petrovic, A., Take, A., Walstein, K., Singh, P., Rondelet, A., Bird, A.W., and Musacchio, A. (2017). CDK-regulated dimerization of M18BP1 on a Mis18 hexamer is necessary for CENP-A loading. eLife *6*, e23352. https://doi.org/10.7554/eLife.23352.
29. McKinley, K.L., and Cheeseman, I.M. (2014). Polo-like kinase 1 licenses CENP-A deposition at centromeres. Cell *158*, 397–411. https://doi.org/10.1016/j.cell.2014.06.016.
30. Stankovic, A., Guo, L.Y., Mata, J.F., Bodor, D.L., Cao, X.J., Bailey, A.O., Shabanowitz, J., Hunt, D.F., Garcia, B.A., Black, B.E., et al. (2017). A Dual Inhibitory Mechanism Sufficient to Maintain Cell-Cycle-Restricted CENP-A Assembly. Mol. Cell *65*, 231–246. https://doi.org/10.1016/j.molcel.2016.11.021.
31. Blomen, V.A., Májek, P., Jae, L.T., Bigenzahn, J.W., Nieuwenhuis, J., Staring, J., Sacco, R., van Diemen, F.R., Olk, N., Stukalov, A., et al. (2015). Gene essentiality and synthetic lethality in haploid human cells. Science *350*, 1092–1096. https://doi.org/10.1126/science.aac7557.
32. Stellfox, M.E., Nardi, I.K., Knippler, C.M., and Foltz, D.R. (2016). Differential Binding Partners of the Mis18alpha/beta YIPPEE Domains Regulate Mis18 Complex Recruitment to Centromeres. Cell Rep. *15*, 2127–2135. https://doi.org/10.1016/j.celrep.2016.05.004.
33. Wang, J., Liu, X., Dou, Z., Chen, L., Jiang, H., Fu, C., Fu, G., Liu, D., Zhang, J., Zhu, T., et al. (2014). Mitotic regulator Mis18beta interacts with and specifies the centromeric assembly of molecular chaperone holliday junction recognition protein (HJURP). J. Biol. Chem. *289*, 8326–8336. https://doi.org/10.1074/jbc.M113.529958.
34. Conti, D., Verza, A.E., Pesenti, M.E., Cmentowski, V., Vetter, I.R., Pan, D., and Musacchio, A. (2024). Role of protein kinase PLK1 in the epigenetic maintenance of centromeres. Science *385*, 1091–1097. https://doi.org/10.1126/science.ado5178.
35. Parashara, P., Medina-Pritchard, B., Abad, M.A., Sotelo-Parrilla, P., Thamkachy, R., Grundei, D., Zou, J., Spanos, C., Kumar, C.N., Basquin, C., et al. (2024). PLK1-mediated phosphorylation cascade activates Mis18 complex to ensure centromere inheritance. Science *385*, 1098–1104. https://doi.org/10.1126/science.ado8270.
36. Cutts, E.E., Taylor, G.C., Pardo, M., Yu, L., Wills, J.C., Choudhary, J.S., Vannini, A., and Wood, A.J. (2021). A commercial antibody to the human condensin II subunit NCAPH2 cross-reacts with a SWI/SNF complex component. Wellcome Open Res. *6*, 3. https://doi.org/10.12688/wellcomeopenres.16482.1.
37. Evans, R., O'Neill, M., Pritzel, A., Antropova, N.A.S., Green, T., Žídek, A., Bates, R., Blackwell, S., et al. (2021). Protein complex prediction with AlphaFold-Multimer. Preprint at bioRxiv. https://doi.org/10.1101/2021.10.04.463034.
38. Jumper, J., Evans, R., Pritzel, A., Green, T., Figurnov, M., Ronneberger, O., Tunyasuvunakool, K., Bates, R., Žídek, A., Potapenko, A., et al. (2021). Highly accurate protein structure prediction with AlphaFold. Nature *596*, 583–589. https://doi.org/10.1038/s41586-021-03819-2.
39. Lee, B.G., Merkel, F., Allegretti, M., Hassler, M., Cawood, C., Lecomte, L., O'Reilly, F.J., Sinn, L.R., Gutierrez-Escribano, P., Kschonsak, M., et al. (2020). Cryo-EM structures of holo condensin reveal a subunit flip-flop mechanism. Nat. Struct. Mol. Biol. *27*, 743–751. https://doi.org/10.1038/s41594-020-0457-x.
40. Hassler, M., Shaltiel, I.A., Kschonsak, M., Simon, B., Merkel, F., Thärichen, L., Bailey, H.J., Macošek, J., Bravo, S., Metz, J., et al. (2019). Structural Basis of an Asymmetric Condensin ATPase Cycle. Mol. Cell *74*, 1175–1188.e9. https://doi.org/10.1016/j.molcel.2019.03.037.
41. Lee, B.G., Rhodes, J., and Löwe, J. (2022). Clamping of DNA shuts the condensin neck gate. Proc. Natl. Acad. Sci. USA *119*, e2120006119. https://doi.org/10.1073/pnas.2120006119.

42. Shaltiel, I.A., Datta, S., Lecomte, L., Hassler, M., Kschonsak, M., Bravo, S., Stober, C., Ormanns, J., Eustermann, S., and Haering, C. H. (2022). A hold-and-feed mechanism drives directional DNA loop extrusion by condensin. Science *376*, 1087–1094. https://doi.org/10.1126/science.abm4012.

43. French, B.T., Westhorpe, F.G., Limouse, C., and Straight, A.F. (2017). Xenopus laevis M18BP1 Directly Binds Existing CENP-A Nucleosomes to Promote Centromeric Chromatin Assembly. Dev. Cell *42*, 190–199. e10. https://doi.org/10.1016/j.devcel.2017.06.021.

44. Yoshida, M.M., Kinoshita, K., Aizawa, Y., Tane, S., Yamashita, D., Shintomi, K., and Hirano, T. (2022). Molecular dissection of condensin II-mediated chromosome assembly using in vitro assays. eLife *11*, e78984. https://doi.org/10.7554/eLife.78984.

45. Elbatsh, A.M.O., Kim, E., Eeftens, J.M., Raaijmakers, J.A., van der Weide, R.H., García-Nieto, A., Bravo, S., Ganji, M., Uit de Bos, J., Teunissen, H., et al. (2019). Distinct Roles for Condensin's Two ATPase Sites in Chromosome Condensation. Mol. Cell *76*, 724–737.e5. https://doi.org/10.1016/j.molcel.2019.09.020.

46. Kong, M., Cutts, E.E., Pan, D., Beuron, F., Kaliyappan, T., Xue, C., Morris, E.P., Musacchio, A., Vannini, A., and Greene, E.C. (2020). Human Condensin I and II Drive Extensive ATP-Dependent Compaction of Nucleosome-Bound DNA. Mol. Cell *79*, 99–114.e9. https://doi.org/10.1016/j.molcel.2020.04.026.

47. Eeftens, J.M., Bisht, S., Kerssemakers, J., Kschonsak, M., Haering, C.H., and Dekker, C. (2017). Real-time detection of condensin-driven DNA compaction reveals a multistep binding mechanism. EMBO J. *36*, 3448–3457. https://doi.org/10.15252/embj.201797596.

48. Ochoa, D., Jarnuczak, A.F., Viéitez, C., Gehre, M., Soucheray, M., Mateus, A., Kleefeldt, A.A., Hill, A., Garcia-Alonso, L., Stein, F., et al. (2020). The functional landscape of the human phosphoproteome. Nat. Biotechnol. *38*, 365–373. https://doi.org/10.1038/s41587-019-0344-3.

49. Neitzel, H., Neumann, L.M., Schindler, D., Wirges, A., Tönnies, H., Trimborn, M., Krebsova, A., Richter, R., and Sperling, K. (2002). Premature chromosome condensation in humans associated with microcephaly and mental retardation: a novel autosomal recessive condition. Am. J. Hum. Genet. *70*, 1015–1022. https://doi.org/10.1086/339518.

50. Trimborn, M., Bell, S.M., Felix, C., Rashid, Y., Jafri, H., Griffiths, P.D., Neumann, L.M., Krebs, A., Reis, A., Sperling, K., et al. (2004). Mutations in microcephalin cause aberrant regulation of chromosome condensation. Am. J. Hum. Genet. *75*, 261–266. https://doi.org/10.1086/422855.

51. Yoshida, M.M., Kinoshita, K., Shintomi, K., Aizawa, Y., and Hirano, T. (2024). Regulation of condensin II by self-suppression and release mechanisms. Mol. Biol. Cell *35*, ar21. https://doi.org/10.1091/mbc.E23-10-0392.

52. Higashi, T.L., Eickhoff, P., Sousa, J.S., Locke, J., Nans, A., Flynn, H.R., Snijders, A.P., Papageorgiou, G., O'Reilly, N., Chen, Z.A., et al. (2020). A Structure-Based Mechanism for DNA Entry into the Cohesin Ring. Mol. Cell *79*, 917–933.e9. https://doi.org/10.1016/j.molcel.2020.07.013.

53. Yu, Y., Li, S., Ser, Z., Kuang, H., Than, T., Guan, D., Zhao, X., and Patel, D. J. (2022). Cryo-EM structure of DNA-bound Smc5/6 reveals DNA clamping enabled by multi-subunit conformational changes. Proc. Natl. Acad. Sci. USA *119*, e2202799119. https://doi.org/10.1073/pnas.2202799119.

54. García-Nieto, A., Patel, A., Li, Y., Oldenkamp, R., Feletto, L., Graham, J.J., Willems, L., Muir, K.W., Panne, D., and Rowland, B.D. (2023). Structural basis of centromeric cohesion protection. Nat. Struct. Mol. Biol. *30*, 853–859. https://doi.org/10.1038/s41594-023-00968-y.

55. Li, Y., Haarhuis, J.H.I., Sedeño Cacciatore, Á., Oldenkamp, R., van Ruiten, M.S., Willems, L., Teunissen, H., Muir, K.W., de Wit, E., Rowland, B.D., et al. (2020). The structural basis for cohesin-CTCF-anchored loops. Nature *578*, 472–476. https://doi.org/10.1038/s41586-019-1910-z.

56. Cutts, E.E., Tetiker, D., Kim, E., and Aragon, L. (2025). Molecular mechanism of condensin I activation by KIF4A. EMBO J. *44*, 682–704. https://doi.org/10.1038/s44318-024-00340-w.

57. Wang, M., Robertson, D., Zou, J., Spanos, C., Rappsilber, J., and Marston, A.L. (2025). Molecular mechanism targeting condensin for chromosome condensation. EMBO J. *44*, 705–735. https://doi.org/10.1038/s44318-024-00336-6.

58. Huis In 't Veld, P.J., Wohlgemuth, S., Koerner, C., Müller, F., Janning, P., and Musacchio, A. (2022). Reconstitution and use of highly active human CDK1:Cyclin-B:CKS1 complexes. Protein Sci. *31*, 528–537. https://doi.org/10.1002/pro.4233.

59. Carette, J.E., Raaben, M., Wong, A.C., Herbert, A.S., Obernosterer, G., Mulherkar, N., Kuehne, A.I., Kranzusch, P.J., Griffin, A.M., Ruthel, G., et al. (2011). Ebola virus entry requires the cholesterol transporter Niemann-Pick C1. Nature *477*, 340–343. https://doi.org/10.1038/nature10348.

60. Schindelin, J., Arganda-Carreras, I., Frise, E., Kaynig, V., Longair, M., Pietzsch, T., Preibisch, S., Rueden, C., Saalfeld, S., Schmid, B., et al. (2012). Fiji: an open-source platform for biological-image analysis. Nat. Methods *9*, 676–682. https://doi.org/10.1038/nmeth.2019.

61. Zivanov, J., Nakane, T., Forsberg, B.O., Kimanius, D., Hagen, W.J., Lindahl, E., and Scheres, S.H. (2018). New tools for automated high-resolution cryo-EM structure determination in RELION-3. eLife *7*, e42166. https://doi.org/10.7554/eLife.42166.

62. Kimanius, D., Dong, L., Sharov, G., Nakane, T., and Scheres, S.H.W. (2021). New tools for automated cryo-EM single-particle analysis in RELION-4.0. Biochem. J. *478*, 4169–4185. https://doi.org/10.1042/BCJ20210708.

63. Pettersen, E.F., Goddard, T.D., Huang, C.C., Meng, E.C., Couch, G.S., Croll, T.I., Morris, J.H., and Ferrin, T.E. (2021). UCSF ChimeraX: Structure visualization for researchers, educators, and developers. Protein Sci. *30*, 70–82. https://doi.org/10.1002/pro.3943.

64. Rohou, A., and Grigorieff, N. (2015). CTFFIND4: Fast and accurate defocus estimation from electron micrographs. J. Struct. Biol. *192*, 216–221. https://doi.org/10.1016/j.jsb.2015.08.008.

65. Zheng, S.Q., Palovcak, E., Armache, J.P., Verba, K.A., Cheng, Y., and Agard, D.A. (2017). MotionCor2: anisotropic correction of beam-induced motion for improved cryo-electron microscopy. Nat. Methods *14*, 331–332. https://doi.org/10.1038/nmeth.4193.

66. Mendes, M.L., Fischer, L., Chen, Z.A., Barbon, M., O'Reilly, F.J., Giese, S. H., Bohlke-Schneider, M., Belsom, A., Dau, T., Combe, C.W., et al. (2019). An integrated workflow for crosslinking mass spectrometry. Mol. Syst. Biol. *15*, e8994. https://doi.org/10.15252/msb.20198994.

67. Cox, J., and Mann, M. (2008). MaxQuant enables high peptide identification rates, individualized p.p.b.-range mass accuracies and proteome-wide protein quantification. Nat. Biotechnol. *26*, 1367–1372. https://doi.org/10.1038/nbt.1511.

68. Tighe, A., Johnson, V.L., and Taylor, S.S. (2004). Truncating APC mutations have dominant effects on proliferation, spindle checkpoint control, survival and chromosome stability. J. Cell Sci. *117*, 6339–6353. https://doi.org/10.1242/jcs.01556.

69. Tighe, A., Staples, O., and Taylor, S. (2008). Mps1 kinase activity restrains anaphase during an unperturbed mitosis and targets Mad2 to kinetochores. J. Cell Biol. *181*, 893–901. https://doi.org/10.1083/jcb.200712028.

70. Ghetti, S., Burigotto, M., Mattivi, A., Magnani, G., Casini, A., Bianchi, A., Cereseto, A., and Fava, L.L. (2021). CRISPR/Cas9 ribonucleoprotein-mediated knockin generation in hTERT-RPE1 cells. Star Protoc. *2*, 100407. https://doi.org/10.1016/j.xpro.2021.100407.

71. Okada, M., and Fukagawa, T. (2006). Purification of a protein complex that associates with chromatin. Protocol Exchange. https://doi.org/10.1038/nprot.2006.417.

72. Müller, F., and Bange, T. (2023). Identification of N-degrons and N-recognins using peptide pull-downs combined with quantitative mass spectrometry. Methods Enzymol. *686*, 67–97. https://doi.org/10.1016/bs.mie.2023.02.007.

73. Michalski, A., Damoc, E., Hauschild, J.P., Lange, O., Wieghaus, A., Makarov, A., Nagaraj, N., Cox, J., Mann, M., and Horning, S. (2011). Mass spectrometry-based proteomics using Q Exactive, a high-performance benchtop quadrupole Orbitrap mass spectrometer. Mol. Cell. Proteomics *10*, M111.011015. https://doi.org/10.1074/mcp.M111.011015.

74. Tyanova, S., Temu, T., and Cox, J. (2016). The MaxQuant computational platform for mass spectrometry-based shotgun proteomics. Nat. Protoc. *11*, 2301–2319. https://doi.org/10.1038/nprot.2016.136.

75. Otsu, N. (1979). A Threshold Selection Method from Gray-Level Histograms. IEEE Trans. Syst. Man Cybern. *9*, 62–66. https://doi.org/10.1109/TSMC.1979.4310076.

76. Lord, S.J., Velle, K.B., Mullins, R.D., and Fritz-Laylin, L.K. (2020). SuperPlots: Communicating reproducibility and variability in cell biology. J. Cell Biol. *219*, e202001064. https://doi.org/10.1083/jcb.202001064.

77. Weissmann, F., Petzold, G., VanderLinden, R., Huis In 't Veld, P.J., Brown, N.G., Lampert, F., Westermann, S., Stark, H., Schulman, B.A., and Peters, J.M. (2016). biGBac enables rapid gene assembly for the expression of large multisubunit protein complexes. Proc. Natl. Acad. Sci. USA *113*, E2564–E2569. https://doi.org/10.1073/pnas.1604935113.

78. Shevchenko, A., Tomas, H., Havlis, J., Olsen, J.V., and Mann, M. (2006). In-gel digestion for mass spectrometric characterization of proteins and proteomes. Nat. Protoc. *1*, 2856–2860. https://doi.org/10.1038/nprot.2006.468.

79. Kolbowski, L., Mendes, M.L., and Rappsilber, J. (2017). Optimizing the Parameters Governing the Fragmentation of Cross-Linked Peptides in a Tribrid Mass Spectrometer. Anal. Chem. *89*, 5311–5318. https://doi.org/10.1021/acs.analchem.6b04935.

80. Iacobucci, C., Götze, M., Piotrowski, C., Arlt, C., Rehkamp, A., Ihling, C., Hage, C., and Sinz, A. (2018). Carboxyl-Photo-Reactive MS-Cleavable Cross-Linkers: Unveiling a Hidden Aspect of Diazirine-Based Reagents. Anal. Chem. *90*, 2805–2809. https://doi.org/10.1021/acs.analchem.7b04915.

81. Roehrl, M.H.A., Wang, J.Y., and Wagner, G. (2004). A general framework for development and data analysis of competitive high-throughput screens for small-molecule inhibitors of protein-protein interactions by fluorescence polarization. Biochemistry *43*, 16056–16066. https://doi.org/10.1021/bi048233g.

82. Bepler, T., Morin, A., Rapp, M., Brasch, J., Shapiro, L., Noble, A.J., and Berger, B. (2019). Positive-unlabeled convolutional neural networks for particle picking in cryo-electron micrographs. Nat. Methods *16*, 1153–1160. https://doi.org/10.1038/s41592-019-0575-8.

83. Zhong, E.D., Bepler, T., Berger, B., and Davis, J.H. (2021). CryoDRGN: reconstruction of heterogeneous cryo-EM structures using neural networks. Nat. Methods *18*, 176–185. https://doi.org/10.1038/s41592-020-01049-4.

84. Ashkenazy, H., Abadi, S., Martz, E., Chay, O., Mayrose, I., Pupko, T., and Ben-Tal, N. (2016). ConSurf 2016: an improved methodology to estimate and visualize evolutionary conservation in macromolecules. Nucleic Acids Res. *44*, W344–W350. https://doi.org/10.1093/nar/gkw408.

STAR★METHODS

KEY RESOURCES TABLE

REAGENT or RESOURCE	SOURCE	IDENTIFIER
Antibodies		
Rabbit anti-CAP-H	Novus Biologicals	Cat# NBP1-32573
Rabbit anti-CAP-D3	Bethyl Laboratories	Cat# A300-601A
Rabbit anti-CAP-D3	Bethyl Laboratories	Cat# A300-604A
Rabbit anti-CAP-G2	Bethyl Laboratories	Cat# A300-605A
Rabbit anti-CAP-H2	Bethyl Laboratories	Cat# A302-275A
Mouse anti-CENP-A	Invitrogen	Cat# MA1-20832
Human anti-CREST	Antibodies Incorporated	Cat# 15-234
Rabbit anti-H3S10ph	Abcam	Cat# Ab5176
Mouse anti-Tubulin	Sigma Aldrich	Cat# T5168
Mouse anti-Tubulin	Sigma Aldrich	Cat# T9026
Rat anti-M18BP1	Conti et al.[34]	N/A
Mouse anti-CyclinB1	Santa Cruz	Cat# sc-245
Rabbit anti-CyclinB1	Abcam	Cat# Ab32053
Mouse anti-PCNA	Cell Signalling Technology	Cat# 2586S
Mouse anti-Histone H3	Abcam	Cat# ab10799
Rabbit anti-MCPH1	Cell Signalling Technologies	Cat# 4120
Rabbit anti-GFP	Musacchio Lab	N/A
Goat anti-CENP-C	Musacchio Lab	N/A
Bacterial and virus strains		
Rosetta™(DE3) Competent Cells	Novagen	Cat#70954
DH10EMBacY	Gibco	Cat#10361012
Chemicals, peptides, and recombinant proteins		
Human condensin I-strep	Kong et al.[46]	N/A
Human condensin II-strep	Kong et al.[46]	N/A
Human condensin II ΔCAP-G2	Houlard et al.[19]	N/A
Human condensin II Qloop-strep	Kong et al.[46]	N/A
CAP-G2	Kong et al.[46]	N/A
CAP-H2	Kong et al.[46]	N/A
MBP-MCPH1$_{1\text{-}195}$	Houlard et al.[19]	N/A
MBP-MCPH1$_{196\text{-}435}$	Houlard et al.[19]	N/A
MBP-MCPH1$_{1\text{-}435}$	Houlard et al.[19]	N/A
MBP-M18BP1$_{873\text{-}1132}$	This study	N/A
MBP-M18BP1$_{873\text{-}1132\text{-}4A}$	This study	N/A
MBP-M18BP1$_{983\text{-}1045}$	This study	N/A
MBP-M18BP1$_{983\text{-}1045\text{-}7A}$	This study	N/A
5FAM-MCPH1$_{407\text{-}422}$	GenScript	N/A
5FAM-MCPH1$_{407\text{-}422}$ -phosphoSer417	GenScript	N/A
Sulfo-SDA (Sulfo-NHS-Diazirine)	Sigma-Aldrich	Cat#803340
Cellfectin II	ThermoFisher	Cat# 10362100
Benzonase	Sigma-Aldrich	Cat# E1014
ATP	Sigma-Aldrich	Cat# A1852
Pierce™ Protease Inhibitor Tablets, EDTA-free	ThermoFisher	Cat# A32965
Terrific Broth	ThermoFisher	Cat# 22711022

(*Continued on next page*)

Continued

REAGENT or RESOURCE	SOURCE	IDENTIFIER
AMP-PNP	Roche	Cat# 10102547001
DTT	Thermo Fisher	Cat# 10699530
Iodoacetamide	Sigma-Aldrich	I6125
Trypsin Protease	Pierce	90057
Acetonitrile, LC-MS grade	Sigma-Aldrich	Cat# A955-4
Trifluoroacetic acid (TFA), LC-MS grade	Sigma-Aldrich	Cat# 302031
DMSO	Thermo Fisher	Cat# D2650
β-Octylglucoside (beta-glucopyranoside)	Sigma-Aldrich	Cat# O8001
Tween-20	Sigma-Aldrich	Cat# P9416
CDK1-Cyclin B with CKS1	Huis In 't Veld et al.[58]	N/A
Fugene6	Promega	Cat# E2692
Nocodazole	Sigma	Cat# m1404
Prolong Gold Antifade	Invitrogen	Cat# P36930
ProLong Glass Antifade Mountant with NucBlue	Invitrogen	Cat# P36981
Janelia Fluor HaloTag ligand 646	Promega	Cat# GA1121
Doxycycline	Sigma-Aldrich	Cat# D9891
Puromycin	Sigma-Aldrich	Cat# P9620
Thymidine	Sigma-Aldrich	Cat# T1895
MG132	MilliporeSigma	Cat# 474790
RO-3306	Merck Millipore	Cat# 217699
SNAP-Cell Block	New England Biolabs (NEB)	Cat# S9106S
SNAP-Cell 647	New England Biolabs (NEB)	Cat# S9102S
Janelia Fluor HaloTag Ligand 646	Promega	Cat# GA1121
Phosphatase Inhibitor Cocktail	Sigma	Cat# P0044
DNase I (RNase-free)	Invitrogen (Ambion)	Cat# AM2222
DAPI	Sigma-Aldrich	Cat# D9542
Mowiol	EMD Millipore	Cat# 475904
Triton X-100	Sigma-Aldrich	Cat# T8787
NP-40	Sigma-Aldrich	Cat# 74385
Opti-MEM	Gibco	Cat# 31985070
Critical commercial assays		
ATPase/GTPase Activity Assay Kit	Sigma-Aldrich	Cat#MAK-113
Superose 6 Increase	Sigma-Aldrich	Cat#GE29-0915-98
Superdex 30 Increase 10/300 GL column	Cytiva	GE29219757
Deposited data		
Atomic coordinates of the condensin II-M18BP1 complex	PDB	9F5W
Cryo-EM map of the condensin II-M18BP1 complex	EMDB	EMD-50201
Mass spec proteomics data	PRIDE	PXD051556
Mass spec XL-MS data	PRIDE	PXD051886
Genetic screen	This study	European Nucleotide Archive accession number PRJEB89880
Experimental models: Cell lines		
sf9	GIBCO	Cat#11496015
High Five cells	GIBCO	Cat#B85502
hTERT RPE1	ATCC	CRL-4000
hTERT RPE1 M18BP1-mNeonGreen-FKBP-V	This study	N/A
HeLa CENP-A-SNAP Flp-In T-REx	Pan et al.[28]	N/A

(*Continued on next page*)

Continued

REAGENT or RESOURCE	SOURCE	IDENTIFIER
HeLa Flp-In T-REx CENP-A-SNAP, EGFP-M18BP1, mCherry-MIS18α	Pan et al.[28]	N/A
HeLa Flp-In T-REx CENP-A-SNAP, mNeonGreen-CAPH2, mCherry-M18BP1	This study	N/A
HeLa Flp-In T-REx CENP-A-SNAP, mNeonGreen-CAPH2, mCherry-M18BP1 4A	This study	N/A
HeLa Flp-In T-REx CENP-A-SNAP, EGFP-M18BP1	This study	N/A
HeLa Flp-In T-REx CENP-A-SNAP, EGFP-M18BP1 7A	This study	N/A
HAP1	Carette et al.[59]	N/A
HAP1 CAP-H2-halo-3xHA	This study	N/A
HAP1 CAP-H2-halo-3xHA M18BP1-5A	This study	N/A
HAP1 CAP-H2-halo-3xHA M18BP1-4A	This study	N/A
HAP1 CAP-H2 knockout	Elbatsh et al.[45]	N/A
HAP1 CAP-H knockout	This study	N/A
Oligonucleotides		
M18BP1_DDFF_AAAA_FW_CCTAAGGACGACCACGCCGCT GCCGCCTCCACCACCCCCCTGCAACACCAG	IDT	N/A
M18BP1_DDFF_AAAA_Rv_CGTGGTCGTCCTTAGGCAGC TGTTCCAGGAAC	IDT	N/A
M18BP1_983-1045	GenScript	N/A
M18BP1_983-1045_T993A_S1004A_T1024A_T1025A_ T1035A_S1042A	GenScript	N/A
gRNA M18BP1 5'-TTGTACTGAAAAAATCATCA-3'	IDT	N/A
gRNA CAP-H2 5'CGGTGCTCCCCACTCAGGGC-3'	IDT	N/A
gRNA CAP-H 5'-GGACTCTGTATACATCGGCA-3'	IDT	N/A
siRNA M18BP1 5'-GAAGUCUGGUGUUAGGAAAdTdT-3'	Eurofins	N/A
siRNA CAP-G2 CAPG2-5'CUCUGAAGUUCGAUCAAAUdTdT-3'	Eurofins	N/A
siRNA MCPH1 5'-CUCUCUGUGUGAAGCACCUdTdT-3'	Eurofins	N/A
Recombinant DNA		
pBIG2abc SMC2, 6x His SMC4, CapD2, CapG, CapH 2x strep	Kong et al.[46]	N/A
pBIG2abc SMC2, 6x His SMC4, CapD3, CapG2, CapH2 2x strep	Kong et al.[46]	N/A
pBIG2abc SMC2 Q147L, 6x His SMC4 Q229L, CapD3, CapG2, CapH2 2x strep	Kong et al.[46]	N/A
pBIG2abc SMC2, 6x His SMC4, CapD3, CapH2 2x strep	Houlard et al.[19]	N/A
pLIB CAP-G2 strep	This study	N/A
pLIB CAP-H2	This study	N/A
pETDuet-MBP-M18BP1-8His_873-1132	This study	N/A
pETDuet-MBP-M18BP1-8His_873-1132-4A	This study	N/A
pETDuet-MBP-M18BP1-8His_983-1045	This study	N/A
pETDuet-MBP-M18BP1-8His_983-1045-7A	This study	N/A
pLIB MCPH1 1-195 ybbr strep	Houlard et al.[19]	N/A
pLIB MCPH1 1-435 ybbr strep	Houlard et al.[19]	N/A
pLIB MCPH1 196-435 ybbr strep	Houlard et al.[19]	N/A
pCDNA5 mNeonGreen-CAP-H2, mCherry-M18BP1	This study	N/A
pCDNA5 mNeonGreen-CAP-H2, mCherry-M18BP1 4A	This study	N/A
pCDNA5 EGFP-M18BP1	This study	N/A
pCDNA5 EGFP-M18BP1 7A	This study	N/A
px459-V2	Addgene	Cat# 62988
px330	Addgene	Cat# 42230

(*Continued on next page*)

Continued

REAGENT or RESOURCE	SOURCE	IDENTIFIER
Software and algorithms		
Fiji	Schindelin et al.[60]	N/A
Prism 10	Graphpad	N/A
RELION-3	Zivanov et al.[61]	N/A
RELION-4	Kimanius et al.[62]	N/A
ChimeraX	Pettersen et al.[63]	N/A
CTFFIND4	Rohou and Grigorieff[64]	N/A
MotionCor2	Zheng et al.[65]	N/A
Excel	Microsoft	N/A
Illustrator 2025	Adobe	N/A
ProteoWizard MSConvert	ProteoWizard	v3.0.22314
xiSEARCH	Mendes et al.[66]	v1.7.6.7
MaxQuant	Cox and Mann[67]	v2.6.6.0
xiFDR	Rappsilber Lab	v2.1.5.2
xiVIEW	Rappsilber Lab	https://xiview.org
AlphaFold2	Jumper et al.[38]	https://github.com/deepmind/alphafold
Other		
Quantifoil R1.2/1.3 Cu 300 mesh grids	Quantifoil Micro Tools	Cat#Q3100CR1.3

EXPERIMENTAL MODEL AND STUDY PARTICIPANT DETAILS

Mammalian cell lines

HAP1 cells were cultured in Iscove's modified Dulbecco's medium (Invitrogen) with 10% FBS (Clontech) and 1% penicillin/Streptomycin (Invitrogen) at 37°C.

HeLa Flip-In T-REx cells were maintained in DMEM medium (Pan Biotech) supplemented with 10% tetracycline-free FBS (Pan Biotech), 50 μg/mL Penicillin/Streptomycin (PAN Biotech), and 2 mM L-glutamine (PAN Biotech) at 37°C.

RPE1 cells were maintained in DMEM/F-12 medium (Pan Biotech) supplemented with 10% tetracycline-free FBS (Pan Biotech), and 50 μg/mL Penicillin/Streptomycin (PAN Biotech) at 37°C.

Bacterial expression systems

E. coli Rosetta (DE3) cells were grown using Terrific Broth medium at 37°C.

E. coli DH10EMBacY cells were grown using LB medium at 37°C.

Insect cell expression systems

Spodoptera frugiperda (Sf9) and Trichoplusia ni (High Five) insect cells were grown in Insect-XPRESS Protein-free Insect Cell Medium (Lonza) at 27°C.

METHOD DETAILS

Cell culture

All cells were cultured at 37°C in a 5% CO_2 atmosphere. HAP1 cells were cultured in Iscove's modified Dulbecco's medium (Invitrogen) with 10% FBS (Clontech) and 1% penicillin/Streptomycin (Invitrogen). For the synthetic lethality screens, haploid HAP1 cells were used.[59] For all other experiments using HAP1 cells, diploid cell lines were used. HeLa Flip-In T-REx cells were maintained in DMEM medium (Pan Biotech) supplemented with 10% tetracycline-free FBS (Pan Biotech), 50 μg/mL Penicillin/Streptomycin (PAN Biotech), and 2 mM L-glutamine (PAN Biotech). RPE1 cells expressing endogenously tagged M18BP1-mNeonGreen were maintained in DMEM/F-12 medium (Pan Biotech) supplemented with 10% tetracycline-free FBS (Pan Biotech), and 50 μg/mL Penicillin/Streptomycin (PAN Biotech).

Genome editing

Endogenous mutations were generated in HAP1 cells using CRISPR-Cas9 technology. Oligonucleotides encoding guide RNAs targeting M18BP1 (5′-TTGTACTGAAAAAATCATCA-3′) were cloned into pX459-v2 and co-transfected using FuGENE 6 (Promega) with pUC19 containing a 1528 base pair stretch containing the mutated sequence of the locus of interest and homology arms. To select

clones, cells were treated with 2 μg/μl puromycin for 2 days before picking colonies. Mutations were validated by Sanger sequencing the isolated genomic DNA. Endogenously tagged CAP-H2-Halo-3xHA cells were generated using guide RNAs targeting the C-terminus of CAP-H2 (5'CGGTGCTCCCCACTCAGGGC-3') in pX330 and a repair template in pUC19. These cells were used as a parental cell line to generate M18BP1 mutant lines described above.

CAP-H2 knockout HAP1 cells were generated as previously described.[45] CAP-H knockout HAP1 cells were generated by insertion of a blast cassette using CRISPR-Cas9 technology. Oligonucleotides encoding guide RNAs targeting CAP-H (5'-GGACTCTGTATAC ATCGGCA-3') were cloned into pX459-v2. Knockout cell lines were confirmed by PCR genotyping, Sanger sequencing and immunoblotting.

HeLa CENP-A-SNAP cell lines co-expressing mNeonGreen-CAPH2 and mCherryM18BP1 variants were generated by transfecting HeLa CENP-A-SNAP Flp-In T-REx cells[28] with pcDNA5 plasmids and pOG44 plasmid according to the protocol previously described.[68,69]

RPE1 M18BP1-mNG-FKBP-V knock-in cell line was generated via electroporation of gRNA-Cas9 ribonucleoproteins (RNPs) as previously described.[70] Briefly, $2x10^5$ parental hTERT-RPE1 Flp-In TRex (a gift from Johnathon Pines) were electroporated with 200 ng of donor DNA, 120 pmol Cas9, 1.5 μl Alt-R® CRISPR-Cas9 crRNA (AATGAGAAAATATGATTCCT,100 μM, IDT), 1.5 μl Alt-R® CRISPR-Cas9 tracrRNA (100 μM, IDT) and 1.2 μl of Alt-R® Cas9 Electroporation enhancer (100 μM, IDT) using P3 Primary Cell Nucleofector® 4D Kit and Nucleofector 4D system (Lonza). After electroporation, cells were treated with 1 μM NU7441 for 48 h. Individual clones were isolated using FACS sorting. Genomic DNA of monoclonal cell lines was extracted and the correct in-frame knock-in was confirmed by Sanger sequencing of PCR products spanning the cut and insertion sites (Forward primer: TGCTCTCAAGTGGACAGACT; Reverse primer: ACCTCTGTCATCCTTCTCACCT).

Chromosome spreads

HAP1 cells were treated with 250 ng/μl nocodazole for 1.5 hours and mitotic cells were collected by shake-off. Cells were incubated with 75 mM KCl for 10 minutes at 37°C. Cells were pelleted and resuspended in fixative (methanol: acetic acid, 3:1) and incubated for 10 minutes at room temperature. Finally, cells were resuspended in fixative with DAPI and dropped onto microscope slides before mounting with Prolong Gold (Invitrogen). Spreads were imaged using the Metafer system (Metasystems). Images were then randomized using a homemade ImageJ macro and blindly assigned a phenotype.

Chromatin fractionation

HAP1 cells were treated with 100 ng/μl nocodazole for 14 hours. Mitotic cells were harvested for both the fractionation protocol and whole cell extract (WCE). WCE was processed as for immunoblotting using RIPA buffer (see below). Cells were pelleted, washed once with PBS and resuspended in lysis buffer (20 mM Tris (pH 7.5), 150 mM NaCl, 5 mM $MgCl_2$ 10% glycerol, 0.2% NP-40, 0.5 mM DTT, Protease inhibitors (Roche) and phosphatase inhibitors (Sigma, 1:100) and incubated on ice for 30 minutes. This cell lysate was then centrifuged at 4°C for 5 minutes at 2000 g. The supernatant was separated from the pellet and centrifuged for 20 minutes at 20,000 g to obtain the soluble fraction. The pellet was washed 4 times in lysis buffer before resuspending in lysis buffer plus benzonase nuclease (Millipore, 70746) and incubated at 4°C on rotation for 1 hour before centrifuging for 30 minutes at 20,000 g. The supernatant contains the chromatin fraction. WCE, soluble and chromatin fractions were all quantified by Bradford assay. 10 μg of the chromatin fraction and 20 μg of soluble fraction or WCE were used for immunoblotting.

Immunofluorescence

HAP1 cells were grown on coverslips and then incubated with 400 nM Janelia Fluor HaloTag ligand 646 (Promega) for 30 minutes then washed three times with media and incubated in fresh media for 30 minutes. Cells were fixed with 4% formaldehyde for 10 minutes then permeabilised with PBS containing 0.15% Triton x100 before blocking in PBST (PBS with 0.05% Tween 20) containing 1% BSA for 1 hour. The following antibodies were used: CENPA (MA1-20832, Invitrogen, 1:1000). Secondary antibodies (Molecular Probes, Invitrogen) were used at 1:1000 for 1 hour. Coverslips were mounted with Prolong Glass Antifade Mountant with NucBlue stain (Invitrogen).

For depletion experiments and compensation assays, HeLa cells were seeded on coverslips and transfected with Lipofectamine RNAiMAX (Invitrogen), the appropriate siRNA oligo (20 nM M18BP1 - 5'-GAAGUCUGGUGUUAGGAAAdTdT-3'; 50 nM CAPG2-5'CUCUGAAGUUCGAUCAAAUdTdT-3'; 200 nM MCPH1-5'-CUCUCUGUGUGAAGCACCUdTdT-3') in serum-Free Opti-MEM medium (Gibco). The transfection controls were set up as above but without adding the siRNA oligos. All conditions were fixed 48 hours from transfection. Exogenous protein expression was induced 24h after transfection by adding Doxycycline (Sigma) to the media at a concentration of 50 ng/ml and induction was performed for 24h. To enrich metaphase cells, 9 μM RO-3306 (Merck Millipore) was added to the media 24h after transfection and cells were incubated for 22 h. Then, drugs were washed out with regular DMEM media and released in media containing 50 ng/ml Doxycycline (Sigma-Aldrich) and 10 μM MG132 (MilliporeSigma). Cells were incubated in the new media for 2h before fixation to allow the enrichment of metaphase states.

For the study of the localisation of M18BP1 during the cell cycle, HeLa or RPE1 M18BP1mNG-FKBP-V knock-in cells were asynchronously grown on coverslips and fixed 48h after seeding. The different cell cycle states were identified by using the appropriate markers in immunostaining.

To assess the deposition of the new pool of CENP-A in early G1, HeLa cells were seeded into 12-well dishes and treated with siRNA as described above. 24 hours after transfection, cells were exposed to media containing 50 ng/ml Doxycycline (Sigma-Aldrich) and 2 mM Thymidine (Sigma-Aldrich) and were incubated for 16h to enrich for cells in G1/S states. The following morning, the drugs were washed out, existing CENP-A-SNAP proteins were labelled for 30 min using 10 μM SNAP-Cell Block (NEB) and cells were exposed to media containing 5 μM S-trityl-L-cysteine (STLC - Sigma-Aldrich) and were let progress through S, G2 and arrest in mitosis for 7h. Then, the newly produced CENP-A-SNAP pool was labelled by exposing the mitotic cells to media containing 3 μM SNAP-Cell 647 (NEB) and 5 μM STLC (Sigma-Aldrich) for 30 min. Once the labelling was completed, the mitotic cells were collected by shake-off, the drugs were washed out and cells were plated in 24-well dishes containing coverslips. Cells were allowed to attach to the bottom of the wells and exit mitosis for 2.5h, then were fixed and immunostained.

HeLa and RPE1 cells were fixed using ice-cold MeOH for 1 min, then washed and rehydrated 3 times for 5 min with PBS + 0.1% Tween 20 (PBST). Cells were blocked for 20 min with PBST + 5% BSA (Pan Biotech) and then were incubated in wet chambers overnight in primary antibodies. The following morning, coverslips were washed 3 times for 5 min with PBST and then incubated at room temperature in secondary antibodies for 30 min. Finally, the coverslips were washed 3 times for 5 min with PBST and mounted on microscope slides using Mowiol (EMD Millipore) as the mounting agent. The primary antibodies used for these experiments are the following: CAPD3 (A300-601A, Bethyl Laboratories, 1:500), CENP-C (Musacchio Lab, 1:1000), CREST (SKU:15-234, Antibodies Incorporated, 1:2000), CyclinB1 (sc-245, Santa Cruz Biotechnology, 1:1000), CyclinB1 (ab32053, Abcam, 1:1000), M18BP1 (Musacchio lab, 1:1000), PCNA (2586S, Cell Signalling Technology), α-Ttubulin (T9026, Sigma Aldrich, 1:500). DNA was visualised using DAPI stain (Sigma, 1:10,000). Fluorescently conjugated secondary antibodies were purchased from Jackson ImmunoResearch Laboratories and used in 1:1,000 dilution. All antibodies were diluted in PBST + 1% BSA.

Chromatin purification

For the immuno-precipitation coupled to mass-spectrometry experiments of Figures 1D and S1B, chromatin was purified either from HeLa FlpIn T-REx cells expressing endogenous CENP-A-SNAP and co-expressing Doxycycline inducible GST-EGFP-M18BP1 and mCherryMIS18α or from HeLa T-Rex FlpIn cells co-expressing Doxycycline inducible EGFP and mCherry as control. Cells were seeded in T175 flasks and arrested for 18 hours in media containing 10 μM STLC (Sigma-Aldrich) and 50 ng/ml Doxycycline (Sigma-Aldrich) to arrest them in mitosis and induce the expression of the exogenous proteins. The arrested cells were subsequently treated with 500 nM Reversine (Cayman Chemical Company), 9 μM RO-3306 (Merck Millipore) and 10 μM Roscovitine (AdipoGen Life Sciences) to induce mitotic exit. After 3 h cells were harvested by trypsinisation, pelleted and flash-frozen in liquid Nitrogen.

For the immuno-precipitation experiment of Figure 1E, chromatin was purified either from HeLa FlpIn T-REx cells expressing endogenous CENP-A-SNAP and co-expressing Doxycycline inducible EGFP-M18BP1 and mCherry-MIS18α or from HeLa T-Rex FlpIn cells co-expressing Doxycycline inducible EGFP and mCherry as control. Cells were seeded in 10 cm dishes and arrested for 24h in media containing 5 μM STLC (Sigma-Aldrich) and 50 ng/ml Doxycycline (Sigma-Aldrich) to arrest them in mitosis and induce the expression of the exogenous proteins. Cells were harvested by mitotic shake-off, pelleted and flash-frozen in liquid Nitrogen.

Chromatin was purified following a modified version of the protocol from.[71] The pellets were resuspended in 5 volumes of buffer containing 20 mM HEPES pH 7.7, 200 mM KCl, 5 mM $MgCl_2$, 1 mM TCEP and supplemented with protease inhibitor cocktail (Serva). Cells were lysed by hypotonic swelling for 2 minutes at room temperature and for 10 minutes on ice. At the end of the incubation, 0.1% NP-40 was added to the tube and the content was mixed by inverting. The lysates were spun at 500g for 10 minutes at 4°C. The cytoplasmic fraction contained in the supernatant was removed and flash-frozen in liquid Nitrogen. The pellet, containing low-purity nuclei, was washed twice with washing buffer (buffer as above supplemented with 0.1% NP-40) and spun at 500 g for 10 minutes at 4°C to remove cytoplasmic impurities. The pellet was resuspended in 5 volumes of washing buffer and sonicated in a Bioruptor Plus (Diagenode) for 5 cycles of 30 seconds ON, and 30 seconds OFF at 4°C. 0.1 μL of Benzonase nuclease (Merck) was added per 200 μL of sample and samples were incubated at 37°C for 5 minutes, followed by incubation at 4°C for 1 hour on a rotor. At the end of the incubation, NaCl was added to a final concentration of 420 mM and salt extraction of the chromatin was performed for 1 hour at 4°C on a rotor. Finally, the samples were centrifuged at 18,000 g for 20 minutes at 4°C. The supernatant containing the solubilised, sheared chromatin fraction was flash-frozen in liquid Nitrogen and stored at -80°C.

Co-immunoprecipitation

For the experiment of Figure 2G, HAP1 cells were pelleted, washed with cold PBS and then lysed for 4 hours on rotation at 4°C in TNEN buffer (50 mM Tris pH 7.5, 1 mM EDTA, 150 mM NaCl, 0.1% NP-40, Protease inhibitors (Roche) and phosphatase inhibitors (Sigma, 1:100) supplemented with Ambion DNaseI (Invitrogen, AM2222, 1:100) and Benzonase nuclease (Millipore, 70746, 600 U/ml). After centrifugation at 12,000 rpm for 10 minutes at 4°C, the supernatant was collected and two volumes of TNENG (TNEN buffer supplemented with 10% glycerol) were added. Lysates were quantified by Bradford assay. Protein lysate and Anti-HA magnetic beads (Pierce 88837) were mixed at a ratio of 10:1 (μg:μl) and incubated overnight at 4°C on rotation. Beads were washed three times with wash buffer (50 mM Tris pH 7.5, 1 mM EDTA, 150 mM NaCl, 0.1% NP-40) and proteins were eluted with Laemmli buffer at 95°C for 10 minutes. Co-immunoprecipitation was assessed by immunoblotting.

For the experiment of Figure 1E, 2 mg of purified chromatin from each sample were mixed with 25 μL of GFP-Trap Agarose (ChromoTek) pre-equilibrated with a buffer containing 20 mM HEPES pH 7.7, 20 mM KCl, 300 mM NaCl, 5 mM $MgCl_2$ and 0.01% Tween-20. The tubes were incubated for 1 hour at 4°C with gentle rotation. Then, the tubes were centrifuged for 5 minutes at

2500 g. The supernatant containing the unbound fraction was removed, and the beads were washed 3 times with 250 μL of buffer, with a 5-minute centrifugation at 2500 g between each wash. After the final wash, the proteins were eluted in 50 μL of 2X Laemmli buffer. 10% of the volume of the purified chromatin used for each sample was taken as input controls. Samples were boiled at 95°C for 5 minutes and results were assessed by immunoblotting.

Immunoblotting

Cells were lysed in RIPA buffer (10 mM Tris-Cl (pH 8.0), 1 mM EDTA, 0.2 mM EGTA, 1% Triton X-100, 0.1% sodium deoxycholate, 0.1% SDS and 140 mM NaCl) and quantified by Bradford. 20 μg protein was run on 4-12% Bis-Tris polyacrylamide gels and transferred to PVDF membranes. Membranes were blocked with TBST (TBS and 0.1% Tween 20) and 5% milk for 1 hour. Primary antibodies were diluted in TBST/Milk as follows: CAP-D3 (A300604A, Bethyl Laboratories, 1:500), CAP-G2 (A300-605A, Bethyl Laboratories, 1:500), CAP-H (NBP1-32573, Novus Biologicals, 1:1000), CAP-H2 (A302-275A, Bethyl Laboratories, 1:500 and 1:1000), GFP (Musacchio Lab, 1:500), Histone H3 (ab10799, Abcam, 1:500), MCPH1 (4120, Cell Signalling Technologies, 1:2000), M18BP1 (Musacchio lab, 1:300), Tubulin (T5168, Sigma Aldrich, 1:50,000), α-Tubulin (T9026, Sigma Aldrich, 1:10,000), H3S10ph (Ab5176, Abcam, 1/2000).

Affinity Purification LC-MS/MS and data analysis

Triplicates of immunoprecipitated GFP-M18BP1 and GFP alone were directly digested on beads.[72] The peptides were subsequently separated on an UltiMate™ 3000 HPLC System (ThermoFisher Scientific) using a 90 min gradient from 5-60% acetonitrile with 0.1% formic acid and directly sprayed via a nano-electrospray source in a quadrupole Orbitrap mass spectrometer (Q Exactive™, Thermo Fisher Scientific™).[73]

Data was acquired in a data-dependent mode acquiring one survey scan (MS scan) and subsequently 15 MS/MS scans of the most abundant precursor ions from the survey scan. The mass range was set to m/z 300 to 1600 and the target value to $3x10^6$ precursor ions with a 1.4 Th isolation window. The maximum injection time for purified samples was 28 msec. MS scans were recorded with a resolution of 60.000 and MS/MS scans with 15.000. Unassigned precursor ion charge states and singly charged ions were excluded. To avoid repeated sequencing, already sequenced ions were dynamically excluded for 30 sec. The resulting raw files were processed with the MaxQuant software (version 1.6.14) using N-terminal acetylation, oxidation (M) as variable modifications and carbamidomethylation (C) as fixed modification. Label-free quantification was enabled. A false discovery rate cut-off of 1% was applied at the peptide and protein levels and as well on the site decoy fraction.[67] The MaxQuant proteingroups.txt output table was then further processed in Perseus (version 1.6.50).[74] Contaminants and reverse hits were removed. To obtain a list of confident interaction partners proteins were filtered for quantification in at least 2 replicates out of 3 replicates. Missing values were imputed with a downshift of 1.8 and a width of 0.3. The cut-off lines for the volcano plot were set to p-value < 0.01 and S0=2.

Synthetic lethality screen

Synthetic lethality screens were carried out as previously described.[31] In brief, haploid cell lines were infected with gene-trap retroviruses which, when integrated in a disruptive (sense) orientation into gene introns, can create a knock-out. By culturing for 12 days, cells with a gene knockout important for cell viability will be depleted from the population and cells in which the virus integrates in a non-disruptive (anti-sense) orientation will survive. As disruptive and non-disruptive integrations occur at similar frequencies, the ratio of insertions in the surviving population indicates whether a gene is important for cell fitness in the specified genetic background. To determine this ratio, cells were harvested and fixed in fix buffer I (BD biosciences). G1 haploid cells, defined by DAPI intensity, were sorted out by flow cytometry on a BD FACSAria Fusion. Genomic DNA was isolated and LAM-PCR carried out to identify insertion sites by sequencing on a Illumina NovaSeq SP with 100bp single reads. Insertion sites were mapped using standard procedures,[31] with some changes. In summary, the unique reads were aligned against the hg38 human genome using Bowtie, allowing for no more than one mismatch. Subsequently, these reads were assigned to protein-coding genes using the longest open reading frame transcript and excluding overlapping regions that cannot be attributed to a single gene. The count of unique alignments was conducted within intronic regions spanning from the transcription start site to the stop codon. A Benjamini-Hochberg false discovery rate–corrected binomial test was employed (FDR-corrected P value cutoff 0.05) to identify the overrepresentation of genes in either the sense or antisense orientation of gene-trap insertions. Additionally, the significance of genes after genetic perturbation (*ΔCAP-H*) compared to wild type control cells was evaluated using a bidirectional Fisher's exact test across four independent control datasets (FDR-corrected p-value cutoff 0.05).

Microscopy and image analysis

Cells from Figures 5B, S5A, S6B, S6E, S7I, and S8D were imaged on a DeltaVision Elite deconvolution microscope (GE Healthcare, UK), equipped with an IX71 inverted microscope (Olympus, Japan), a UPLSAPO x100/1.40NA oil objective (Olympus) and a pco.edge sCMOS camera (PCO-TECH Inc., USA). Cells from Figures 4A, S5G, S7B, and S7F were imaged on a spinning disk confocal device on the 3i Marianas system equipped with an Axio Observer Z1 microscope (Zeiss), a CSU-X1 confocal scanner unit (Yokogawa Electric Corporation, Tokyo, Japan), x100/1.4NA oil objective (Zeiss), and Orca Flash 4.0 sCMOS Camera (Hamamatsu). All the images were acquired as z-sections at 0.2 μm.

HAP1 cells from Figures 3A and S5F were imaged on an AxioObserver Z1 (Zeiss) microscope with an x63 oil immersion objective and z stacks of 0.2 μm. Images of HAP1 cells were converted to maximum intensity projections for analysis. Other acquired images were converted into sum intensity projections, exported, and converted into 8-bit using ImageJ.[60] Quantification of the chromatin signal was performed on Fiji using a script for semiautomated processing. Briefly, Regions of interest (ROIs) were established by segmenting the chromatin DAPI signal via Otsu thresholding.[75] Applying those ROIs to the respective fluorescent channels yielded mean protein signal intensities. Correction for background intensity was done by subtracting from the mean protein intensity the mean intensity from the border region around the chromatin. This border region was bounded to the inside by the ROI and to the outside by the ROI, which was slightly enlarged by repeated binary dilation. Absolute signal intensities were calculated by multiplying background-corrected mean intensities with chromatin ROI area. Data was normalised using Excel (Microsoft) and plotted using GraphPad Prism (GraphPad) software. Data was visualised as violin plots in Prism 8. For each sample, the median value of each repeat was superimposed to the violin plots as described in the SuperPlots methodology.[76] The figures were arranged using Adobe Illustrator software.

Inter-kinetochore distances were measured manually in Fiji software. DAPI and CREST channels from deconvolved images were used to identify kinetochores of the same bi-oriented sister chromatids pair. Measurements were performed in Z-stacks where both the sister kinetochores were visible, and the distance between the CREST signals was measured using a straight line. 10 inter-kinetochore distances were randomly measured for each cell and the average value was used in the final plotting.

Protein expression and purification

Human condensin I, condensin II, condensin II sub-complexes, and condensin II Q-loop mutant (See key resources table) were assembled into biGBac vectors as described previously.[19,46,77] Recombinant bacmids were generated via Tn7 transposition in DH10EMBacY cells and transfected into Sf9 cells. Virus-containing supernatant was harvested after 3 days and futher amplified in Sf9 cells for 3 additional days. For protein expression, amplified virus was used to infect High Five insect cells. Cells were harvested by centrifugation 3 days post-infection. Cell pellets were resuspended in 20 mM HEPES pH 8, 300 mM KCl, 5 mM $MgCl_2$, 1 mM DTT, 10% glycerol, supplemented with 1 Pierce EDTA-free protease inhibitor tablet (Thermo Scientific) and 25 U/mL Benzonase (Sigma). Cells were lysed using a dounce homogenizer followed by sonication for 5 minutes (10 seconds on and 20 seconds off), and clarified by centrifugation for 40 minutes at 4 degrees using Beckman Coulter F20 rotor at 20k RPM. Clarified lysates were loaded onto a Strep-Tactin XT column (IBA Lifesciences), washed with lysis buffer, and eluted with the same buffer supplemented with 50 mM biotin (Sigma). Protein fractions were pooled and diluted 3-fold in Buffer A (20 mM HEPES pH 8, 5 mM $MgCl_2$, 5% glycerol, 1 mM DTT). The diluted sample was loaded onto a HiTrap Heparin HP column (GE Healthcare), washed with Buffer A containing 250 mM NaCl, and eluted with Buffer A containing 500 mM NaCl. Finally, protein was further purified by size exclusion chromatography using Superose 6 Increase 16/600 (GE Healthcare) equilibrated in 20 mM HEPES pH 8, 300 mM KCl, 5 mM $MgCl_2$, 1 mM DTT, 10% glycerol. Fractions containing purified complexes were pooled, concentrated and flash frozen in liquid Nitrogen. MBP-MCPH1$_{1\text{-}195}$, MBP-MCPH1$_{196\text{-}435}$, and MBP-MCPH1$_{1\text{-}435}$ were purified as described in Houlard et al.[19] MBP-M18BP1$_{873\text{-}1132}$, MBP-M18BP1$_{873\text{-}1132\text{-}4A}$, MBP-M18BP1$_{983\text{-}1045}$ and MBP-M18BP1$_{983\text{-}1045\text{-}7A}$ were expressed in Rosetta (DE3). Cells were grown in Terrific Broth media at 37 degrees. Upon reaching OD of about 4, cells were induced for 2 hrs at 30 degrees, then centrifuged and flash frozen in liquid nitrogen. Cells were resuspended in HEPES pH 7.5, NaCl 200 mM, glycerol 10% and DTT 2mM, and lysed by sonication on ice at 60% amplitude, 30 second on and 30 seconds off for a total of 5 minutes. After centrifugation the supernatant was injected on a His Trap column and eluted with increasing concentration of Imidazole. The His tag purification was followed by a MBP affinity purification and finally a size exclusion column (Superdex 200 16/600). Phosphorylation of M18BP1 was obtained by treating the purified protein overnight at 4 degrees with CDK1:Cyclin-B:CKS1 complexes in presence of 2 mM ATP and 10 mM $MgCl_2$ as described in Huis in 't Veld P. J. et al.[58]

Sulfo-SDA crosslinking reaction and peptide preparation for crosslinking MS

Condensin II and MBP-M18BP1$_{873\text{-}1132}$ (previously treated with CDK1:Cyclin-B:CKS1) at 1.5 μM were incubated with AMPPNP at 1mM concentration and reacted with sulfo-NHS-diazirine (sulfo-SDA, Thermo Scientific) at 0.5/1/1.5mM. The crosslinked protein material was then separated on a 4-12% bis-tris SDSPAGE gel (life technologies) and the bands corresponding to the crosslinked protein complex were excised and processed by in-gel digestion.[78] Briefly, the proteins were reduced with 20mM dithiothreitol (DTT, thermo scientific) and alkylated with 55mM iodoacetamide (IAA, merck millipore) prior to digestion with trypsin (Pierce). Peptides were then recovered and desalted with C18 StageTips (Empore) and crosslinked peptide pairs were enriched by size exclusion chromatography (SEC)[79] using a superdex 30 increase column (Cytiva) equilibrated with 30% acetonitrile, 0.1% trifluoroacetic acid. 50μl fractions were collected and early eluting fractions were taken for LC-MS.

Sulfo-SDA Crosslinking MS acquisition

Approximately 1μg of peptides of each fractionwere injected for each liquid chromatographymass spectrometry (LC-MS) acquisition. The LC-MS platform consisted of a Vanquish Neo system (ThermoFisher Scientific) connected to an Orbitrap Eclipse Tribrid mass spectrometer (ThermoFisher Scientific) equipped with a FAIMS Pro Duo device operating under Tune 3.5.3886. Mobile phases consisted of 0.1% v/v formic acid in water (mobile phase A) and 0.1% formic acid in 80% acetonitrile/water v/v (mobile phase B). Samples were dissolved into 4% mobile phase B. The FAIMS Pro Duo device was set to standard resolution with a carrier gas

flow of 4.6L/min. The samples were separated on an EASY-Spray PepMap Neo column (75 μm x 50 cm) (ThermoFisher Scientific). Peptides were separated on 110 minute gradients designed to match the hydrophobicity of the various SEC fractions, with linear separation gradients from 20%-40%B in 77 minutes (earliest fraction, most hydrophobic), down to 11%B to 35%B (latest fraction, least hydrophobic).

MS1 spectra were acquired with a resolution of 120,000 and automated gain control target set to 250% and 50ms maximum injection time. Source RF lens was set to 35%. Dynamic exclusion was set to single count in 60 seconds. The duty cycle was set to 2.5 seconds. A precursor charge filter was set to z=3-7. Precursors were selected based on a data-dependent decision tree strategy prioritizing charge states 4-7 and subjected to stepped HCD fragmentation with normalized collision energies of 20, 27, 30.[79] MS2 scans were acquired with a normalized gain control target of 750% with maximum injection time of 250ms and an orbitrap resolution of 60,000. For each SEC fraction, multiple injections were carried out with multiple FAIMS control voltages, with the first 3 injections being performed at -45V, -55V and -65V separately, and, if possible, a final injection with a 2 CV combination of -40/-75V each with a duty cycle of 15 seconds.

For further data for proteomics analysis, 200ng of each fraction was injected with a 60 minute gradient (linear 2%-20% B in 37 minutes, then 10 minutes to 35% B prior to wash in 95%B). FAIMS control voltage was set to -45. MS1 resolution was set to 120,000 and automated gain control of 100%, with a maximum injection time of 25 ms. In this case charge states 2-5 were selected for fragmentation in the linear ion trap in rapid mode.

Sulfo-SDA Crosslinking MS data analysis

Raw files were converted to mgf format using ProteoWizard MSconvert (version 3.0.22314). A recalibration of the MS1 and MS2 m/z was conducted based on high-confidence (<1% false discovery rate) linear peptide identifications using xiSEARCH (version 1.6.745). Crosslinking MS database search was performed in xiSEARCH (version 1.7.6.7)[66] on a database comprising human condensin II, M18BP1, contaminants from protein purifications, and common mass spec contaminants derived from MaxQuant[67] searched with 4 missed tryptic cleavages. Precursor mass error tolerance was set to 3ppm and MS2 error tolerance to 5ppm. The search included methionine oxidation, asparagine deamidation, SDA loop link (+82.04186484Da), hydrolized SDA (+100.0524) as variable modifications. Site-specific phosphorylation at T993 of M18BP1 was defined as a variable modification. The SDA crosslinker was defined as cleavable.[80] The search was set to account for noncovalent gas-phase associations. Prior to FDR estimation, search results were filtered to only include peptide spectra matches with at least 2 crosslinker-containing fragments on both peptides. Results were filtered to 5% FDR at the residue pair level and 10% at the protein pair level using xiFDR (version 2.1.5.2) and the "boost" feature to optimize thresholds at the lower error levels was enabled to maximise heteromeric crosslinks. Results were exported in mzIdentML format and uploaded to xiview.org for visualization. Pseudobonds files were downloaded and visualized on the structural model using chimera X version 1.6.1 (Figure S4).

Analysis of phosphorylation in crosslinking MS sample

In order to identify the *in vitro* phosphosites of M18BP1, all Sulfo-SDA crosslinking MS acquisitions and proteomics injections of the same sample were analysed with MaxQuant 2.6.6.0 with the same database used for the crosslinking MS search, with the addition of CDK1. Oxidation of methionine, acetylation of N-termini and phosphorylation of serine and threonine were set as variable modifications. The phosphosites table is included in Table S3.

Analytical size exclusion chromatography

Condensin II at final concentration of 10 μM was mixed with $M18BP1_{873-1132}$ (WT or DDFF to AAAA mutant version) at final concentration 20 μM. 50 μL of the reaction mixture were injected onto a 2.4 ml Superose 6 Increase gel filtration column (GE Healthcare) equilibrated in 20 mM TRIS pH 8.5, 150 mM NaCl, 5mM $MgCl_2$, 5% (v/v) Glycerol and 2 mM DTT. 50 μL fractions were collected and analysed by SDS–PAGE using 4–12% NuPAGE Bis-Tris gels (Invitrogen). The gels were run in MOPS buffer at 200 V for 45 min and stained with Instant- Blue Coomassie protein stain (Abcam).

ATPase assay

ATPase activities were measured using the ATPase/GTPase Activity Assay Kit (MAK-113, Sigma-Aldrich) according to the manufacturer's instruction. $M18BP1_{873-1132}$ used in these assays was phosphorylated by CDK1:Cyclin-B:CKS1 and ATP with overnight treatment. Condensin II wild type or ATPase deficient mutant were first incubated with $M18BP1_{873-1132}$ (previoulsy treated with CDK1:Cyclin-B:CKS1). After that, the complexes were run over analytical gel filtration to remove residual ATP from phosphorylation reactions. The complex was then diluted to 200 nM with Assay Buffer (20 mM Tris pH 8.5, 50 mM NaCl, 5 mM $MgCl_2$, 5% (w/v) glycerol, 2 mM ATP, DTT 2mM). Reactions in presence of phosphorylated 4A mutant version of $M18BP1_{873-1132}$, were performed by mixing with condensin II wild type or ATPase deficient mutant after running analytical gel filtration in separate runs, as the 4A mutant does not coelute with condensin II. For the experiments containing DNA, a 10 fold excess of dsDNA to protein was used. 20 μL of the reaction mixture containing the diluted proteins were incubated for 30 min at 20°C. Then, 100 μL of malachite green reagent was added into each reaction well and incubated for 10 min. After that, the absorbance at 620 nm was measured, proportional to the enzyme activity present. Concentration of free phosphate produced [Pi] (μM) was derived from the standard curve previously determined, and the

ATP hydrolysis rate calculated using the fourmula: Enzyme Activity = [P_i (μM) x R_v]/[S_v x T]; where R_v is the reaction volume, S_v is the sample volume added to the well and T is the reaction time expressed in minutes.

Fluorescence anisotropy protein binding assays

Peptides used in fluorescence anisotropy assays were synthesised by Genscript and are shown in Table S1. The concentration of 5-FAM wild type MCPH1$_{407-422}$ was determined using the 5-FAM extinction coefficient of 83,000 (cmM)–1 at 493 nm. Non-labelled peptides had TFA removed to less than 1 % and were accurately quantified using Genscript's amino acid analysis service. All peptides were solubilised in DMSO and diluted to a working concentration in FP assay buffer (20 mM Tris pH 8.5, 200 mM NaCl, 1 mM DTT, Tween20 0.08%, BSA 0.5mg/mL).

FP competition assays with non-phosphorylated MCPH1 were performed using 0.3μM of 5FAM-labelled MCPH1$_{407-424}$ peptide, with or without 0.8 μM of condensin II pentamer and with 8 μM of MBP-MCPH1$_{1-195}$, MBP-MCPH1$_{196-435}$, MBP-MCPH1$_{1-435}$ or MBP-M18BP1$_{873-1132}$ in a total volume of 40 μl in half-area black plates (Constar). The plate was incubated at room temperature for 20 min, before being read with an Omega plate reader (BMG Labtech) at 5 min intervals and monitored to ensure binding had reached equilibrium. Each plate was read three times, and three replicates were performed. The buffer only background was subtracted and mean and standard deviation was calculated.

FP Binding assays with phosphorylated or unphosphorylated 5-FAM-labelled MCPH1$_{407-424}$ peptide to condensin II was performed using 0.3 μM peptide, with increasing concentration of condensin II ranging from 20 nM to 5 μM.

Fluorescence anisotropy phospho-M18BP1 competition assay

FP Competition assays with phosphorylated and unphosphorylated M18BP1 and a MCPH1$_{407-424}$ – condensin II complex were performed using 0.3 μM of 5-FAM-labelled MCPH1$_{407-424}$ peptide and 0.6 μM of condensin II pentamer. The complex of condensin II – 5-FAM-labelled MCPH1$_{407-424}$ was incubated with increasing concentrations (30 nM to 15 μM) of a MBP-M18BP1 fragment consisting of residues 983 to 1045. In parallel a mutant version of MBP-M18BP1 was used where potential phosphorylation sites were replaced with alanine (M18BP1$_{983-1045}$-7A: T993A – S1004A – T1023A – T1024A – S1026A – T1035A – S1042A). CDK1-cyclin B treatment with ATP and $MgCl_2$ was performed to phosphorylate these sites. After overnight treatment, the excess of ATP and CDK1-cyclin B were removed by analytical gel filtration using a Superose 6 Increase 10/300 GL column equilibrated with the assay buffer. To ensure consistent treatment of the samples, the phosphorylation reaction and subsequent purification were performed on both M18BP1$_{983-1045}$-WT and M18BP1$_{983-1045}$-7A.

All assays were measured at 25°C in Corning 384-well Black Round Bottom well plates. Three independent measurements were collected and averaged for each point of the binding isotherms. The dissociation constant (K_D and K_{D2}) values and standard error of the mean were calculated in Graphpad Prism, using all data points from three independent experiments. FP data was fit using equations for direct binding and directly competitive binding.[81]

Cryo-EM sample preparation and data acquisition

For the preparation of cryo-EM samples (Figure S2), purified condensin II and M18BP1$_{873-1132}$ (previously treated with CDK1) were incubated with 2 mM AMP-PNP for 30 min. The sample was then run on a glycerol (10-25%) and glutaraldehyde (0-0.2%) gradient by ultracentrifugation with a Sw60 rotor set on a G-force of 29k for 16hrs at 4 degrees. After the GraFix fixation, the complex was again separated from the aggregates and washed off the glycerol on a Superose 6 Increase 10/300 GL column equilibrated in TRIS pH 8.5, NaCl 150 mM, DTT 2mM, 0.03% beta-glucopyranoside and 0.03% Tween20. The peak fractions corresponding to the right molecular weight were pooled and concentrated. The freshly purified condensin II – M18BP1$_{873-1132}$ complex (OD280 = 0.5) was applied to Quantifoil R1.2/1.3 300-mesh copper holey carbon grids, previously glow-discharged using a GloQube (Quorum) set at 30 mA for 60 seconds. Grids were blotted for 3.5 s under 100% humidity at 4℃ before being plunged into liquid ethane using a Vitrobot Mark IV (Thermo Scientific). Micrographs were acquired as EER movies on a Titan Krios G4 (Thermo Scientific) transmission electron microscope operated at 300 kV with a Falcon 4i (Thermo Scientific) direct electron detector and Selectris X (Thermo Scientific) energy filter set with slit width of 10 eV. EPU (Thermo Scientific) software was used for automated data collection following standard procedures. A magnification of 105x was used for imaging, yielding a pixel size of 1.2 Å on images. The defocus range was set from -0.5 μm to -2 μm. Each micrograph was dose-fractionated to 50 frames, with a total dose of about 50 e-/Å^2.

Cryo-EM image processing

The detailed image processing and statistics are summarized in Figures S2 and S3 and Table 1. Motion correction was performed using the Relion's own implementation of the MotionCorr2 program,[65] and the CTF parameters of the micrographs were estimated using the CTFFIND program.[64] Most steps of image processing were performed using RELION-3 or RELION-4.[61,62] Initially, particle picking was performed by using the Laplacian-of-Gaussian blob detection method in RELION-3. Class averages representing projections in different orientations were selected from the initial reference-free 2D classification and further used for 3D initial model and 3D classification in RELION. Particles aligning in the best 3D classes were used for Topaz[82] training and autopicking. Extracted particles were binned 3 times and subjected to 2D classification and 3D classification. The selected classes from 3D classification were subjected to 3D auto refinement followed by Bayesian polishing. Polished particles were used for three rounds of 3D classification with alignment. Finally, we performed 3D classification without local search that yielded to a final set of 49k particles. Selection of

particles was used for 3D auto-refine job and final map was post-processed to correct for modulation transfer function of the detector and sharpened by applying a negative B factor, manually set to -150. A soft mask was applied during post processing to generate FSC curves to yield a map of average resolution of 7 Å. The RELION local resolution procedure was used to estimate local resolution for the map that resulted in a resolution range between 5 and 11 Å. Attempts at Multibody refinement or CryoDRGN[83] were made to increase local resolution of subunits. However, both programs showed a continuous motion among subunits that could not be resolved in local minima, hence limiting the overall resolution of the map.

Structure and sequence analysis

Sequence conservation predictions were made with ConSurf.[84] AlphaFold structure prediction was performed using AlphaFold2-multimer and was executed using a locally installed version of AlphaFold2.[38] This local version of AlphaFold2-multimer operates with V3 model parameters and utilizes default arguments. The databases employed for the prediction in the step of Multiple Sequence Alignment (MSA) generation are as follows: Uniref30 (UniRef30_2021_03), Uniref90 (downloaded on 04/02/2023), UniProt (downloaded on 03/02/2023), PDB_mmcif (downloaded on 04/02/2023), PDB_seqres (downloaded on 04/02/2023), PDB70 (version 06/09/2014), mgnify (version 05/2022), and BFD.

The multimer prediction was utilized for full length proteins (CAP-G2 with MCPH1 or M18BP1). The highest-ranked structures are displayed in the figures, accompanied by the Predicted Alignment Error (PAE) plot of the highest-ranked. Images for figures were generated using UCSF ChimeraX.[63]

QUANTIFICATION AND STATISTICAL ANALYSIS

Statistical analysis was performed in Prism 8. All cell biology experiments were repeated at least 3 times to attain statistical significance. We used the Mann-Whitney test for experiments comparing two conditions (Figures 3B, 4C, S5D–S5F, S5H–S5K, S6F, S6G, and S8E–S8G), and the Kruskall-Wallis test coupled with Dunn's multiple comparisons for experiments comparing 3 or more conditions (Figures 3E, 4F, S5B, S6C, S6D, S7C, S7G, and S7J). All statistically significant comparisons are represented on figures by asterisks. Error bars of chromosome spreads experiments (Figure 3D) represent mean ± s.d. Fluorescence Anisotropy assay (Figure 4D) results are presented as mean ± s.d from three independent experiments. Binding curves for Fluorescence Anisotropy assays (Figures 5A and S8A) are derived fitting equations in Prism10 for direct binding and directly competitive binding[81] from three independent experiments.